SYNTHESIS AND CHARACTERIZATION OF KCC-1 PREPARED FROM WASTE MATERIAL FOR HEAVY METAL REMOVAL

HERMA DINA BINTI SETIABUDI

RESEARCH VOTE NO:
RDU170331

Faculty of Chemical & Natural Resources Engineering

UNIVERSITI MALAYSIA PAHANG

2019

ACKNOWLEDGEMENTS

I would like to acknowledge Universiti Malaysia Pahang for funding this research activity through RDU170331 and Chemical Engineering Laboratory, FKKSA UMP for equipment and facilities available. I also would like to extend my gratitude to team members who always help and gave advice during this research period. Thank you to my students that works out the research plan accordingly.

ABSTRACT

SYNTHESIS AND CHARACTERIZATION OF KCC-1 PREPARED FROM WASTE MATERIAL FOR HEAVY METAL REMOVAL

(Keywords: Lead, Adsorption, Fibrous Silica Nanosphere (KCC-1), Waste Material, Response Surface Methodology (RSM))

Lead (Pb(II)) is one of the most toxic metals found in water bodies through industrial activities which can cause severe hazardous impacts to living organisms even at trace levels. Therefore, several methods for lead removal have been investigated, including the adsorption process. Regarding the selection of adsorbent, fibrous silica nanosphere (KCC-1) has attracted considerable attention owing to its high surface area and fibrous silica morphology. However, owing to the high cost of the commercial silica precursor, utilization of rice husk ash (RHA) (SiO_2 = 95.44%) as alternative silica source seems to be a promising approach and the application of amine functionalization will enhance its adsorption capacity. Thus, the main objective of this study is to synthesize and characterize KCC-1(RHA) for Pb(II) removal. The characterization analyses showed that the synthesized KCC-1(RHA) consists of fibrous silica morphology with high surface area ($S_{BET,\ KCC\text{-}1(RHA)}$ = 220 m^2/g, $S_{BET,\ NH_2/KCC\text{-}1(RHA)}$ = 274 m^2/g) comparable with KCC-1 synthesized from commercial silica source, indicating the successful formation of KCC-1 structure from RHA. The influences of prominent parameters (initial concentration (X_1), adsorbent dosage (X_2) and time (X_3)) on Pb(II) removal was evaluated by RSM, and the optimal conditions were achieved at X_1 = 322.06 mg/L, X_2 = 2.4 g/L and X_3 = 117 min, with 74.50% of Pb(II) removal from aqueous solution. The experimental data were analyzed using Langmuir, Freundlich, Temkin, and Dubinin-Redushkevich isotherm models, and were found to follow Langmuir isotherm model with maximum adsorption capacity of 26.954 mg/g and high correlation coefficient (R^2 = 0.9934), implying monolayer adsorption occurred on the homogenous surface of the adsorbent. Pseudo-first order, Pseudo-second order, and Elovich kinetic models were tested with the experimental data, and Pseudo-second order kinetic model was best fitted the adsorption process, indicating that the adsorption process most likely controlled by the chemisorption process and the rate of reaction is directly proportional to the number of active sites on the surface of adsorbent. The regeneration and reusability studies revealed that KCC-1(RHA) performs good adsorption-desorption for five cycles with a moderate reduction in the percentage of Pb(II) removal. This study revealed that RHA demonstrated great potential as silica precursor of KCC-1 for excellent Pb(II) adsorption from aqueous solution.

Key researchers: Herma Dina Setiabudi, Syarifah Abd Rahim, Noor Sabrina Ahmad Mutamim, Nurul Aini Mohamed Razali

E-mail : herma@ump.edu.my; Tel. No. : 09-5492836; Vote No. : RDU170331

ABSTRAK

Sintesis dan Analisis KCC-1 Disediakan Dari Bahan Buangan Untuk Penyingkiran Logam Berat

(Kata Kunci: Plumbum, Penjerapan, Nanosfera Silika Berserat (KCC-1), Bahan Buangan, Kaedah Respons Permukaan (RSM)

Plumbum (Pb(II)) adalah salah satu logam yang sangat toksik yang terdapat di dalam air melalui aktiviti perindustrian yang boleh membahayakan organisma hidup walaupun di tahap yang susah untuk di kesan. Oleh itu, beberapa kaedah untuk menyingkirkan plumbum telah dikaji, termasuklah proses penjerapan. Berkenaan dengan pemilihan penjerap, nanosfera silika berserat (KCC-1) telah menarik perhatian ramai kerana mempunyai luas permukaan yang tinggi dan morfologi silika berserat. Walau bagaimanapun, disebabkan oleh kos silika komersial yang tinggi, penggunaan abu sekam padi (RHA) (SiO_2 = 95.44%) sebagai sumber alternatif merupakan pendekatan yang berkesan dan penggunaan fungsian amina akan meningkatkan kapasiti penjerapan. Oleh itu, objektif utama kajian ini adalah untuk mensintesis dan mencirikan KCC-1(RHA) untuk pengingkiran Pb(II). Analisa pencirian menunjukkan bahawa KCC-1 yang disistesis mempunyai morfologi silika berserabut dengan luas permukaan yang tinggi ($S_{BET,\ KCC\text{-}1(RHA)}$ = 220 m^2/g, $S_{BET,\ NH_2/KCC\text{-}1(RHA)}$ = 274 m^2/g) setanding dengan KCC-1 yang disintesis menggunakan silika komersial, menunjukkan pembentukan struktur KCC-1 yang berjaya dari RHA. Pengaruh parameter yang penting (kepekatan awal (X_1), dos penjerap (X_2), dan masa (X_3)) kepada penyingkiran Pb(II) telah di nilai dengan menggunakan RSM, dan keadaan optimum telah dicapai pada X_1 = 322.06 mg/L, X_2 = 2.4 g/L dan X_3 = 117 min dengan 74.50% Pb(II) telah disingkirkan daripada larutan akueus. Data eksperimen dianalisis menggunakan model isoterma Langmuir, Freundlich, Temkin, dan Dubini-Redushkevich, dan didapati mengikut isoterm Langmuir dengam kapasiti penjerapan maksimum 26.954 mg/g dan pekali korelasi yang tinggi (R^2 = 0.9934), menunjukkan jerapan monolapisan berlaku pada permukaan homogen penjerap. Model kinetik tertib pseudo-pertama, tertib pseudo-kedua, dan Elovich diuji dengan data eksperimen, dan model kinetik tertib pseudo-kedua adalah paling sesuai dengan proses penjerapan, menunjukkan bahawa proses penjerapan dikawal oleh proses kimia dan kadar tindak balas berkadar terus dengan bilangan tapak aktif pada permukaaan penjerap. Kajian penjanaan dan kebolehgunaan semula menunjukkan bahawa NH_2/KCC-1(RHA) telah menunjukkan prestasi yang baik semasa lima kitaran penjerapan-penyahjerapan dengan penurunan yang sederhana dalam peratus penyingkiran Pb(II). Kajian ini membuktikan RHA mempunyai potensi yang besar sebagai sumber silica KCC-1 untuk penyingkiran Pb(II) yang cekap dari larutan akueus.

Penyelidik utama: Herma Dina Setiabudi, Syarifah Abd Rahim, Noor Sabrina Ahmad Mutamim, Nurul Aini Mohamed Razali

E-mail : herma@ump.edu.my; Tel. No. : 09-5492836; Vote No. : RDU170331

TABLE OF CONTENT

DECLARATION

TITLE PAGE

ACKNOWLEDGEMENTS **ii**

ABSTRACT **iii**

ABSTRAK **iv**

TABLE OF CONTENT **v**

LIST OF TABLES **viii**

LIST OF FIGURES **ix**

LIST OF SYMBOLS **x**

LIST OF ABBREVIATIONS **xi**

CHAPTER 1 INTRODUCTION **1**

1.1 Research Background 1

1.2 Problem Statement 3

1.3 Objectives 3

1.4 Scope of Research 3

CHAPTER 2 LITERATURE REVIEW **5**

2.1 Heavy Metal 5

2.2 Lead (Pb(II)) 6

2.3 Methods Available for Lead (Pb(II)) Removal 7

2.3.1 Chemical treatment 7

2.3.2 Physical treatment 9

2.4 Adsorption Study 12

2.5 Utilization of Waste Material as Silica Source 16
2.5.1 Fly Ash 16
2.5.2 Sugarcane bagasse 17
2.5.3 Rice Husk Ash 18
2.6 Silica-based Materials 20
2.6.1 Mesoporous Silica 20
2.6.2 Fibrous Silica Nanosphere (KCC-1) 24
2.7 Optimization study 26
2.7.1 Theory and steps for RSM application 27
2.7.2 Application of Response Surface Methodology 31
2.8 Summary 31

CHAPTER 3 METHODOLOGY 33

3.1 Material 33
3.2 Preparation of adsorbent 33
3.2.1 Extraction of sodium silicate from RHA (Na_2SiO_3-RHA) 33
3.2.2 Preparation of KCC-1 34
3.2.3 Characterization of synthesized KCC-1 34
3.3 Batch Adsorption 35
3.4 Experimental design and optimization 36

CHAPTER 4 RESULTS AND DISCUSSION 37

4.1 Characterization of KCC-1 37
4.2 Optimization of Pb(II) removal onto KCC-1(RHA) by Response Surface Methodology (RSM) 39
4.3 Adsorption Kinetics 43
4.4 Adsorption Isotherm 45

4.5 Regeneration and Reusability 48

CHAPTER 5 CONCLUSION **50**

5.1 Conclusion 50

5.2 Recommendation for Future Work 51

REFERENCES **52**

ACHEVEMENTS **64**

LIST OF TABLES

Table 2.1	Toxicities of heavy metal, the maximum contaminant level (MCL) and Maximum Permissive Limit (MPL)	5
Table 2.2	Toxicity of Pb(II) to human	6
Table 2.3	Comparison physisorption and chemisorption	14
Table 2.4	Advantages and disadvantages of adsorbents	15
Table 2.5	Physical composition of Fly ash	16
Table 2.6	Chemical composition of Fly Ash	17
Table 2.7	Physical properties of sugarcane bagasse ash	18
Table 2.8	Chemical Composition of sugarcane bagasse ash	18
Table 2.9	Composition of Rice husk	19
Table 2.10	Physical properties RHA	19
Table 2.11	Chemical properties RHA	19
Table 2.12	Characteristics of KCC-1	25
Table 2.13	Differences between response surface methodology (RSM) and one-variable-at-a-time technique	27
Table 2.14	Summary for properties alternative silica source	32
Table 3.1	List of material used	33
Table 4.1	Experimental design and results obtained for Pb(II) removal onto KCC-1(RHA).	39
Table 4.2	ANOVA analysis of Pb(II) removal onto KCC-1(RHA).	40
Table 4.3	Kinetic parameters for Pb(II) removal onto KCC-1(RHA).	45
Table 4.4	Isotherm models for Pb(II) adsorption onto KCC-1(RHA).	47
Table 4.5	Comparison of Pb(II) adsorption capacity of several types of silica absorbent.	47

LIST OF FIGURES

Figure 2.1	Mechanism of adsorption and desorption	13
Figure 2.2	Illustration of physisorption and chemisorption	14
Figure 2.3	Different pore structure of mesoporous material	21
Figure 2.4	Structural design of, (A) MCM-41 and (B) MCM-48	21
Figure 2.5	Illustrated mechanism of MCM-41	22
Figure 2.6	The structure of SBA-15	23
Figure 2.7	The structure of MSN	24
Figure 2.8	KCC-1 strucure	25
Figure 2.9	Quadratic response surface plot profile	30
Figure 4.1	XRD pattern of KCC-1(RHA) and KCC-1(C)	37
Figure 4.2	FTIR spectra of KCC-1(RHA) and KCC-1(C)	38
Figure 4.3	TEM image of (A) KCC-1(C) and (B) KCC-1(RHA)	38
Figure 4.4	Pareto chart and *p*-value for Pb(II) removal onto KCC-1(RHA).	41
Figure 4.5	3D surface plots of percentage Pb(II) removal onto KCC-1(RHA) predicted from the quadratic model: (A) initial concentration – adsorbent dosage interaction, (B) initial concentration – time interaction, and (C) adsorbent dosage – time interaction.	43
Figure 4.6	Adsorption-desorption for removal of Pb(II) onto KCC-1(RHA).	48
Figure 4.7	FTIR spectra of KCC-1(RHA) before and after five cycles of adsorption-desorption towards Pb(II) removal.	49

LIST OF SYMBOLS

q_t	Values of Pb(II) adsorbed at time, *t* (mg/g)
q_e	Values of Pb(II) adsorbed at equilibrium (mg/g)
k_2	Pseudo-second order adsorption (g/mg.min)
k_1	Rate constant of pseudo-second order adsorption (L
β	Desorption constant during the experiment (g/mg)
α	Adsorption rate constant (mg/(g.min))
n	Empirical constant
C_e	Pb(II) concentration at equilibrium (mg/L)
K_L	Langmuir constant (L/mg)
K_F	Freundlich constant ((mg/g)(L/mg)$^{1/n}$))
B	Temkin constant
A	Temkin equilibrium binding constant (L/g)
K_{DR}	Dubinin-Radushkevich constant (mol^2/kj^2)
ε	Polanyi potential (J/mol)
R	Gas constant (8.314 J/mol·K)
T	Absolute temperature
R_L	Dimensionless constant separation factor
Y	Predicted respond
β_0	Offset term
$\beta_1, \beta_2, \beta_3$	Linear terms
$\beta_{11}, \beta_{22}, \beta_{33}$	Quadratic terms
$\beta_{12}, \beta_{13}, \beta_{23}$	Interaction term
R^2	Regression coefficient

LIST OF ABBREVIATIONS

BET	Surface area analyser
CTAB	Cetyltriammonium bromide
FTIR	Fourier transform infrared spectroscopy
ICPMS	Inductively coupled plasma mass spectrometry
KCC-1	Fibrous silica nanosphere
RHA	Rice Husk Ash
RSM	Response surface methodology
XRD	Wide-angle powder X-ray diffraction
XRF	X-ray fluorescence

CHAPTER 1

INTRODUCTION

1.1 Research Background

Heavy metals, such as Pb(II), Cu(II), and Zn(II), are the main toxic pollutants in industrial wastewater, and they have been found to be the major contaminants of surface and ground water, causing various diseases and disorders. Among heavy metals, lead (Pb(II)) is one of the most toxic metals found in water bodies through industrial activities such as metal plating facilities, mining operations, fertilizer industries, tanneries, batteries, paper and pesticides industry. This metal mainly originates from the feedstock, corrosion products of the equipment and pipes, process chemical additives, and materials used in the processes (Beddri & Ismail, 2007). The exposure to the Pb(II) in the body through inhalation and ingestion of food or water cause a serious disease and permanent damage to human health such as nervous system, kidney, fatal brain, and circulatory system (Begum, 2015). Besides, Pb(II) also affected the aquatic life such as change in physiology, biochemistry, behaviour, and reproduction (Parmar & Thakur, 2013). According to the World Health Organization (WHO) and United States Environmental Protection Agency (USEPA), the maximum permissive limit (MPL) and maximum contaminant level (MCL) of Pb(II) concentration are only less than 0.01 mg/L and 0.006 mg/L, respectively (United States Environmental Protection Agency, 1979; World Health Organization, 1984). Thus, the concentration of Pb(II) in petrochemical wastewater must be reduced before discharge to the surrounding using a suitable removal technique.

The study of Pb(II) removal has been reported using various techniques such as chemical precipitation (Chen, 2009; Kavak, 2013), ion exchange (Al-Enezi, 2004; Saruchi & Kumar, 2016), membrane filtration (Taylor et al., 2011; Yurekli et al., 2017), coagulation-flocculation (Ferniza-garcía et al., 2017; Moi et al., 2011), flotation (Ghazy

et al., 2008; Mohammed et al., 2013) and adsorption (Guo et al., 2017; Sharahi & Shahbazi, 2017). Among the stated techniques, adsorption gained much attention due to the low cost, minimum production of chemical/biological sludge, simplicity, and flexible design (Kalantari et al., 2014; Vijayalakshmi et al., 2017).

During the past few years, a considerable number of researches have been devoted towards the application of mesoporous silica as contemporary alternative adsorbent for Pb(II) adsorption from wastewater owing to its promising physical and chemical properties such as controlled pore sizes, narrow pore sizes distribution, and large surface area (Byoun et al., 2018; Guo et al., 2017; Javadian et al., 2017; McManamon et al., 2012; Singh & Polshettiwar, 2016). Large surface area of mesoporous silica improves the accessibility of adsorbate to the adsorbent, while, narrow pore sizes distribution and controlled pore sizes will aid the adsorption of the large molecule (McManamon et al., 2012). Furthermore, the presence of a silanol group is beneficial for adsorption process as the presence of negative charge results in higher amount of available sites for the adsorption of molecule ions (Singh & Polshettiwar, 2016).

In 2010, the new mesoporous silica, which is fibrous silica nanosphere (KCC-1) has been developed by King Abdullah University of Science and Technology (KAUST) Catalyst Centre (Bayal et al., 2016). KCC-1 attracted considerable attention for its wide applications such as catalysis (Hamid et al., 2017), drug delivery (Bayal et al., 2016) and CO_2 capture-conversion (Singh & Polshettiwar, 2016) owing to its high surface area, fibrous surface morphology with the dendrimeric silica fibres, wide pore diameter, high mechanical, and thermal stability (Dong et al., 2014, 2015; Rahman et al., 2016). Owing to its excellent properties, it is attempted to study the Pb(II) removal performance of KCC-1 adsorbent. However, the commercial silica precursor such as tetraethyl orthosilicate ($SiC_8H_{20}O_4$, TEOS) and sodium silicate (Na_2SiO_3) for KCC-1 synthesis is relatively expensive, thus the utilization of silica-rich waste material as an alternative silica source would minimize the production cost of KCC-1.

In recent years, the utilization of silica-rich waste as alternative low-cost materials to substitute the commercial silica precursor has attracted considerable attention among the researchers. Rice husk ash (RHA) is one of the major agricultural wastes in Malaysia with the production of 408,000 metric tonnes per year (Noor & Rohasliney, 2012). RHA has been demonstrated to be a potentially feasible resource for synthesizing silica-based materials owing to its high silica content (94.95%) (Patil et al., 2014). For the time being, RHA was disposed at the open area which resulted in the environmental pollution. Thus,

the utilization of rice husk ash as silica source (Na_2SiO_3-RHA) would increase the economic value to these agricultural commodities, help to reduce the cost of waste disposal, and thus can reduce the environmental pollution.

1.2 Problem Statement

Lead (Pb(II)), which exists in industrial wastewater, has been acknowledged as one of the most hazardous heavy metals and may cause numerous health problems even at low concentration (Pam et al., 2018; Isabella & Pérez, 2015). Adsorption has become one of the popular technique in the removal of heavy metal due to the low cost, minimized chemical/biological sludge, and simplicity/flexible design (Kalantari et al., 2014; Vijayalakshmi et al., 2017).

With regards to the adsorbent material, a new type of mesoporous silica material which is known as fibrous silica nanosphere (KCC-1) is expected to have good adsorption performance owing to its high surface areas, fibrous surface morphology, wide pore diameter, high mechanical and thermal stability (Dong et al., 2014, 2015; Rahman et al., 2016). However, the commercial silica precursor for KCC-1 synthesis is relatively expensive, thus the utilization of silica-rich waste material as an alternative silica source would minimize the production cost of the KCC-1.

1.3 Objectives

The objectives of this study are:

i. To synthesize and characterize the KCC-1(RHA)
ii. To study the optimum condition of Pb(II) removal onto KCC-1(RHA) by Response Surface Methodology (RSM).
iii. To study the kinetic, isotherm and reusability studies of Pb(II) removal onto KCC-1(RHA).

1.4 Scope of Research

The scopes of this study are:

Work scopes for objective 1

- Preparation of KCC-1(RHA) using sodium silicate from RHA and compared with KCC-1 prepared from commercial sodium silicate (Na_2SiO_3) (KCC-1(C)).
- Determination of the physical and chemical properties of synthesized KCC-1 using transmission electron microscopy (TEM), x-ray diffraction (XRD), Fourier transform infrared spectroscopy (FTIR) and surface area analyser (BET).

Work scope for objective 2

- Investigation of the optimum condition of Pb(II) removal onto KCC-1(RHA) using Response Surface Methodology (RSM) under three independent variables including initial concentration (50 – 400 mg/L), adsorbent dosage (0.5 – 5.0 g/L) and time (0 – 140 min).

Work scopes for objective 3

- Investigation of the kinetic study of Pb(II) removal onto KCC-1(RHA) using Pseudo-first order, Pseudo-second order, and Elovich kinetic models.
- Investigation of the isotherm study of Pb(II) removal onto KCC-1(RHA) using Langmuir, Freundlich, Temkin, and Dubinin-Redushkevich isotherm models.
- Investigation of the reusability studies of the Pb(II) removal onto KCC-1(RHA) at optimum condition.

CHAPTER 2

LITERATURE REVIEW

2.1 Heavy Metal

Heavy metals such as cadmium, mercury, arsenic, chromium, zinc, copper and lead found in industrial wastewater can be harmful to human and aquatic life even at very low concentration (Abadin et al., 2007). Heavy metals that were non-degradable can affects the human and aquatic life by accumulating in soils, sediments and certain tissues of bodies or by indirectly transfer to the food chain (Almalih et al., 2015). In addition, heavy metals prevent the growth of phytoplankton by inhibiting photosynthesis in water plants, caused chromosomal and tissue damage in terrestrial plants (Akinbayo Akinbiyi, 2000). Table 2.1 describes the toxicity of heavy metals to the human, the maximum contaminant level (MCL) from United States Environmental Protection Agency (USEPA) and Maximum Permissive Limit (MPL) from World Health Organization (WHO). From Table 2.1, it can be concluded that all types of heavy metals have negative effects on human and thus need to be removed from wastewater.

Table 2.1 Toxicities of heavy metal, the maximum contaminant level (MCL) and Maximum Permissive Limit (MPL)

Heavy Metals	**Toxicities**	**MCL (mg/L)**	**MPL (mg/L)**
Arsenic	Skin manifestation, visceral cancel, vascular disease	0.05	0.01
Cadmium	Kidney damage, renal disorder, human carcinogen	0.01	0.003
Chromium	Headache, diarrhoea, nausea, vomiting, carcinogen	0.05	0.05

Copper	Liver damage, Wilson disease, insomnia	0.25	1.0
Nickel	Dermatitis, nausea, chronic asthma, coughing, human carcinogen	0.20	0.02
Zinc	Depression, lethargy, neurological signs and increased thirst	0.80	3.0
Lead	Damage the fatal brain, disease of the kidney, circulatory system, and nervous system	0.006	0.01
Mercury	Rheumatoid arthritis, and disease of the kidneys, circulatory system and nervous system	0.00003	0.001

Sources: (Begum et al., 2015; Parmar & Thakur, 2013; United States Environmental Protection Agency, 1979; World Health Organization, 1984)

2.2 Lead (Pb(II))

Lead (Pb(II)) can often be found in industrial wastewater that originated from the feedstock, corrosion of the equipment and pipes, process chemical additives, catalysts and other materials used in downstream processes of the primary distillation (Beddri & Ismail, 2007). The exposure of the Pb(II) to the body through inhalation and ingestion of food or water will cause serious diseases and permanent damage to human health. Pb(II) mainly affects the nervous system, hematopoietic system, renal, cardiovascular, and reproductive health. Table 2.2 describes the toxicity of Pb(II) to human.

Table 2.2 Toxicity of Pb(II) to human

Human Part	**Toxicity**	**Ref.**
Nervous system	• Hallucination, irritability, headache, muscular tremor, dullness, loss of memory, • Children – delayed growth, decreased intelligent, short-term memory, hearing loss • At high level, permanent brain damage and even death	(Abbaszadeh et al., 2016; Flora et al., 2012; Moyo et al. Guyo, 2013; Salim & Munekage, 2009)
Hematopoietic system	• Forms complexes with oxo-groups in enzymes t effect virtually all steps in the process of haemoglobin synthesis	(Flora et al., 2012; Moyo et al., 2013; Rajput et al., 2015;

	• Reduces the life span of circulating erythrocytes by increasing the fragility of the cell membranes • Anaemia	Salim & Munekage, 2009)
Renal	• Acute nephropathy – decreasing kidney function due to the high level of glucose, amino acids and phosphate in urine • Chronic nephropathy – renal breakdown, hypertension and hyperuricemia	(Flora et al., 2012; Moyo et al., 2013; Yi et al., 2016)
Cardiovascular	• Hypertension, heart disease, cerebrovascular accident, peripheral vascular disease	(Flora et al., 2012; Moyo et al., 2013; Yi et al., 2016)
Reproductive Health	• Men – reduced libido, abnormal spermatogenesis, chromosomal damage, infertility, abnormal prostatic function, change in serum testosterone • Women – infertility, miscarriage, premature membrane rupture, pre-eclampsia, pregnancy hypertension, premature delivery	(Abbaszadeh et al., 2016; Flora et al., 2012; Moyo et al., 2013; Salim & Munekage, 2009; Yi et al., 2016)

From Table 2.2, it can be concluded that Pb(II) is highly dangerous to human. In addition, World Health Organization (WHO) stated that only less than 0.01 mg/L concentration of Pb(II) is allowed in drinking water (World Health Organization, 1984), while Environment Protection Agency (EPA) declared that the presence of Pb(II) is toxic even in a low concentration (McManamon et al., 2012). Thus, owing to the high toxicity of Pb(II), concentration of Pb(II) must be reduced before being discharged to the surrounding using a suitable removal technique.

2.3 Methods Available for Lead (Pb(II)) Removal

The removal of Lead (Pb(II)) from aqueous solution and wastewater has been studied using several treatment processes including chemical and physical treatments. The available techniques for Pb(II) removal will be discussed in subtopic 2.4.1 and 2.4.2.

2.3.1 Chemical treatment

Chemical treatment is the process whereby chemicals are used during wastewater treatment. The chemical precipitation and coagulation-flocculation are the most reported

chemical treatment in Pb(II) removal and these methods will be explained in detail in subtopic 2.4.1.1 and 2.4.1.2.

2.3.1.1 Chemical Precipitation

Chemical precipitation is the most common technology used in removing ionic metals from solution, such as process wastewaters containing toxic metals. Chemical precipitation involved a reaction between heavy metal and chemical in aqueous solution or wastewater and formed insoluble precipitated that can be removed by sedimentation technique (Singh et al., 2017). This method has attract considerable attention in removal of Pb(II) due to the low cost, effective to threat the high concentration of effluent and ease of pH control (Fu & Wang, 2011; Malik et al., 2016; Parmar & Thakur, 2013).

In most chemical precipitation reaction, lime is used as precipitant for removal process due to its relatively low cost. Chen et al. (2009) has reported the used of lime with addition of fly ash as a seed material to enhance lime precipitation before being exposed to the carbon dioxide gas for heavy metal removal. The fly ash-lime-carbonation treatment increased the size of precipitate particles and thus increased the removal of heavy metal. In their study, the percentage removal of Zn(II), Pb(II) and Cr(II) was around 99.37-99.69%. Besides, hydroxide precipitate has also been used in chemical precipitation such as NaOH, $Ca(OH)_2$, KOH, Phosphate, Sulphides, and carbonates. The use of $Ca(OH)_2$ for removal of Pb(II) has been reported by Kavak (2013) with 99.42% of Pb(II) removal at pH of 12, mass of precipitating agent of 0.75 g/L in 30 min precipitation time. The use of hydrogen sulphide (H_2S) was successfully removed 100% of Cu(II), 94% of Zn(II), and 92% of Pb(II) as reported by Alvarez et al. (2007).

Even though the chemical precipitation has high efficiency in removal process, however, it has less attraction to the industry owing to the large amount of chemical used, thus increased the cost for the large-scale treatment process. In addition, since this process required addition of the chemical, thus, generated an excessive amount of sludge and problem in sludge disposal (Malik et al., 2016; Parmar & Thakur, 2013).

2.3.1.2 Coagulation-flocculation

Coagulation-flocculation method is the combination of two methods that commonly used to separate the suspended solids from the water. In brief, coagulation

method involved the addition of coagulant such as aluminium, calcium, or ferric ions into solution, as such flocculation is induced (Parmar & Thakur, 2013). The application of coagulation-flocculation method in Pb(II) removal has been reported in literature. Ferniza-garcia et al. (2017) found that the addition of aluminium electrodes in parallel arrangement as coagulant successfully removed 99.2% of Cu, 81.3% of Cd, and 99.4% of Pb. Besides, the use of aluminium sulfate (alum), polyaluminium chloride (PACI), and magnesium chloride ($MgCl_2$) as coagulant have been reported by Pang et al. (2011). In their study, the maximum Pb(II) removal was achieved at pH of 8.0-9.3 for PACI, 8.7-10.9 for $MgCl_2$, and 6.2-7.8 for alum with Pb(II) removal of 99.1%, 98.4%, and 99%, respectively.

In brief, the coagulation-flocculation treatment has economic feasibility and high efficiency, in spite of that, the cost of chemical is expensive (Kharub, 2012). Moreover, even though it is efficient, the overall disadvantage of chemical treatment is found from the production of sludge at the final stage of the treatment which is pH dependent and brings about disposal problems (Kharub, 2012; Parmar & Thakur, 2013).

2.3.2 Physical treatment

Physical treatment is a removal of substances by physical barrier and forces such as electrical attraction, gravity, and van der Waal forces. Usually, this method does not change the chemical structure of the substance. However, the physical state of the substance might be changed. This method includes membrane filtration process, ion exchange, and adsorption techniques and will be explained in detail in subtopic 2.4.2.1 to 2.4.2.3.

2.3.2.1 Membrane Filtration

Membrane filtration is a process of removing pollutant from suspensions such as inorganic/organic metal ions, microorganism, and turbidity by passing through a selective barrier (membrane) using vacuum or pressure driven (Shon et al., 2008). Membrane filtration with different types of membrane such as ultrafiltration, reverse osmosis, nanofiltration, and electrodialysis, have been widely used in the removal of Pb(II) due to the high efficiency, no phase change, and environmental friendly (Fu & Wang, 2011; Singh et al., 2017).

The use of membrane filtration method was reported by several researchers including Yurekli et al. (2017) on synthesis of zeolite nanoparticles incorporated polysulfone (PSf10) membrane for the removal of lead and nickel. From their study, 77% and 92% of lead and nickel, were successfully removed from the solution. Moreover, in another study, Al-Rashdi et al. (2011) found that the application of nanofiltration (NF) membrane had successfully removed several heavy metals such as Cd(II), Mn(II), Pb(II), As(III) and As(V) with percentage removal of heavy metals around 99.9% for Cu(II) (C_0 = 12,000 ppm), 97% for Cd(II) (initial concentration C_0 = 500 ppm), 98% for Mn(II) (C_o =310 ppm), 84% for Pb(II) (C_o = 0.64 ppm, 89% for As(III), and 93% for As(V) (total arsenic concentration = 600 ppm). Hajdu et al. (2012) reported the application of ultrafiltration technique for Pb(II) removal with Pb(II) removal of 99.8%, thus achieving the drinking water standard by World Health Organization (WHO). In addition, Zhu et al. (2018) found that the application of Al_2O_3-NaA zeolites composite hollow fibre membranes synthesized from solid waste coal fly ash had successfully removed about 99.9% of Pb(II) from synthetic wastewater at 0.1 MPa after 12h of filtration.

Even though membrane filtration was believed to be the efficient method in Pb(II) removal, however, membrane fouling will happen due to the membrane pores blocked with metal ions, thus, lowering the flux and increasing the required energy which leads to high operating cost (Samal et al., 2016). Besides, the sludge generation has also become the drawback of the process (Ahmad et al., 2007; Parmar & Thakur, 2013).

2.3.2.2 Ion Exchange

Ion exchange treatment is a method whereby one or more undesirable contaminants can be removed from water by exchange with another non-objectionable or less objectionable substances. Both the contaminant and the exchanged substance must be dissolved and have the same type (+, -) of electrical charged. The use of ion exchange has several advantages such as high treatment capacity, high removal efficiency, and no adsorbent loss during regeneration process (Ahmad et al., 2007; Fu & Wang, 2011; K. Singh et al., 2017; Wenchao et al., 2016). This can be proved by the high percentage removal of Pb(II) reported in the literature.

Merganpour et al. (2015) studied the removal of Pb(II) in drinking water using a cationic resin, Purolite. In their study, 95.42% of Pb(II) had been successfully removed from drinking water. Moreover, Al-Enezi et al. (2004) reported the removal of heavy

metal from wastewater sludge using ion exchange resin, with 99.9% of heavy metal had been removed successfully. The use of hybrid ion exchange has also been studied by Saruchi and Kumar (2016). In their study, Gum tragacanth-zirconium (IV) tungstoiodophosphate based ion exchange was synthesized and was applied in the removal of rhodamine B and Pb^{2+} from aqueous solution. In their study, the percentage removal of rhodamine B and Pb^{2+} was 97.8% and 98.5% respectively, under 5 g/L of adsorbent dosage, 7.7 of pH, and 10 ppm of initial concentration. Besides the advantages identified, some drawbacks have been reported for this method such as non-selective in operation and highly sensitive to the pH of the solution (Malik et al., 2016).

2.3.2.3 Adsorption

Adsorption is a process of a gas or liquid solute accumulating on the surface of adsorbent (solid or liquid) to form an adsorbate (molecule or atomic film) (Parmar & Thakur, 2013). The use of this method has attract considerable attention in the removal of Pb(II) from aqueous solution due to the interesting advantages of this process which are low cost, minimum chemical and biological sludge, and simplicity and flexibility of design has attracted researchers to use this method (Fu & Wang, 2011; Kalantari et al., 2014; Vijayalakshmi et al., 2017). However, the efficiency of this process depends on the efficiency of the adsorbent (Fu & Wang, 2011).

The use of the adsorption process in the Pb(II) removal has been reported by many researchers. Sharahi and Shahbazi (2017) reported the use of Melamine-based dendrimer amine-modified magnetic nanoparticles (MDA-Fe_3O_4) as adsorbent for adsorption Pb(II) and optimization using response surface methodology. From their study, 85.6% of Pb(II) was removed using MDA-Fe_3O_4 under optimum condition (initial Pb(II) concentration of 110 mg/L, adsorbent dosage of 0.49 g/L and temperature of 30°C). The use of chitosan-functionalized MCM-41-A as adsorbent has been reported by Guo et al. (2017). They found that 99.83% of Pb(II) was successfully removed using chitosan-functionalized MCM-41-A under initial concentration of 100 mg/L, adsorbent dosage of 3 g/L, pH of 6 and in 60 min of the adsorption process. In addition, Lingamdinne et al. (2018) reported the removal of Pb(II) using nickel ferrite-reduced graphene oxide nano-composite (NFRGO) as adsorbent. In their study, 99% of Pb(II) was successfully removed under optimum condition of initial concentration of 18.38 mg/L, adsorbent dosage of 0.55 g/L in 83 min of adsorption process.

From the literature on the removal of Pb(II), adsorption method has attracted considerable attention as compared to the other methods owing to its simplicity in the design and affordable process. According to Thilagavathy and Santhi (2012), adsorption was proved to be the most inexpensive method in wastewater treatment especially in treatment of low concentration solution and in treatment of stringent levels. In addition, the adsorption process also produces high quality of the treated effluent whereby the adsorbent can be regenerated by suitable desorption process.

2.4 Adsorption Study

Adsorption is a transfer of substance from liquid phase to the solid surface, while, desorption is a vice versa of the adsorption, which is the transfer of substance from the surface of the solid back to the liquid phase (Rashed, 2013; Tripathi & Ranjan, 2015). Usually, adsorption involved exothermic reaction due to the release of energy to the surrounding during the process, while desorption involved endothermic reaction due to the absorb of energy. The substance (solute) that bind on the solid surface is called adsorbate, while, the solid that bind by solute is called adsorbent (Rashed, 2013). The adsorption happens when solute (in the liquid phase) accumulate on the active site on the solid surface using mass transfer process through the interaction of liquid-solid intermolecular forces (Tan & Wei, 2008). The surface of the adsorbent can be classed into two which is homogeneous or heterogeneous surface. The homogeneous surface is a surface that has uniform composition or character (constant energy), while, heterogenous is a surface that has non-uniform composition or character (distribute energy). In general, the equilibrium of the process depends on the concentration of adsorbate in the solution. When the adsorbate has higher concentration, the adsorbate concentration on the adsorbent surface to reach equilibrium is also higher (did not exceed adsorbent maximum adsorption capacity). The adsorption-desorption mechanism as illustrated in Figure 2.1.

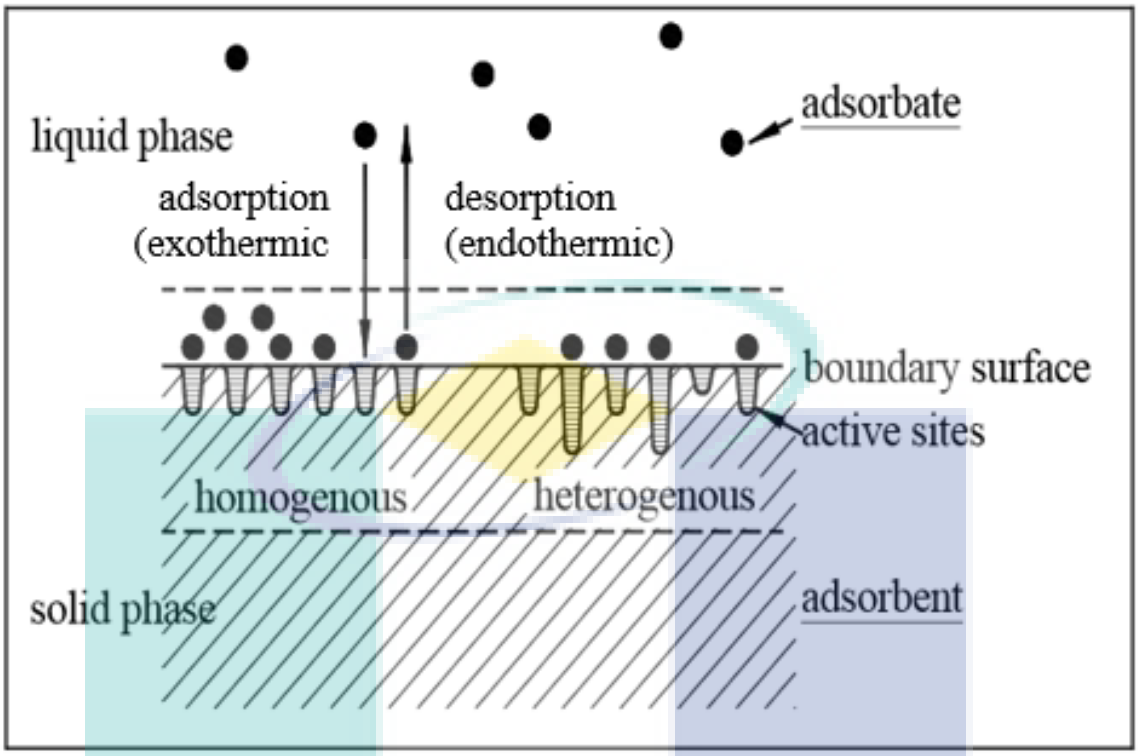

Figure 2.1 Mechanism of adsorption and desorption
Source: (Tan & Wei, 2008)

The adsorption process can be classified into two type which is physical adsorption (physisorption) and chemical adsorption (chemisorption). As illustrated in Figure 2.2, physisorption process involves the attraction of adsorbate to the high surface area of adsorbent by weak bonds (Van der Waals, hydrogen bond and dipole-dipole) and the heat of adsorption was low which slightly greater than the adsorbate transfer heat (Berger & Bhown, 2011). In contrast, chemisorption involves binding of adsorbate on certain site of adsorbent by chemical reaction (ionic bond, covalent bond) with the heat of adsorption equal to the heat of reaction (Berger & Bhown, 2011; Teka & Enyew, 2014). However, there is possibility for both of the adsorption types to occur simultaneously such as physical adsorption will occur at low temperature and may pass into chemisorption as the temperature increased, thus resulted in difficulty to determine the type of adsorption process. The comparison between physisorption and chemisorption are illustrated in Table 2.3.

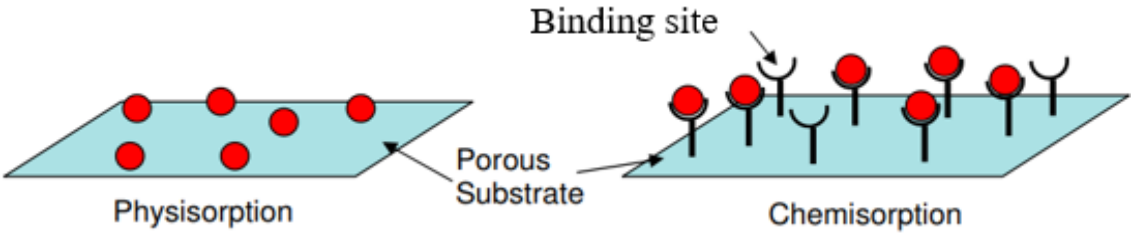

Figure 2.2 Illustration of physisorption and chemisorption

Source: (Berger & Bhown, 2011)

Table 2.3 Comparison physisorption and chemisorption

Physisorption	**Chemisorption**
Van der waals' forces, hydrogen bond and dipole-dipole interactions	Chemical bond formation (covalent bond, ionic bond)
Not specific in nature	Highly specific in nature
Reversible in nature	Irreversible
Low temperature is favourable for adsorption. It decreases with increasing of temperature.	High temperature is favourable for adsorption. It increases with increasing of temperature.
No appreciable activation energy is needed	High activation energy is sometimes needed
Increase with increasing surface area	Increase with increasing surface area
Multimolecular layer on adsorbent surface under high pressure	Unimolecular layer

Sources: (Sarda et al., 2015; Tan & Wei, 2008; Teka & Enyew, 2014; Tripathi & Ranjan, 2015)

The adsorption process has attracted considerable attention among researchers due to the adsorbent can be regenerated, economical, simple and flexible of design (Al-Rashdi et al., 2011; Fu & Wang, 2011; Kalantari et al., 2014; Vijayalakshmi et al., 2017). Besides, this process also produces minimum biological and chemical sludge. However, the efficiency of the adsorption process depends on the adsorbent used. Thus, the choice of suitable adsorbent is crucial in this process.

Adsorbent is a solid that will capture solute onto their active site of the surface. The use of the suitable adsorbent is important in the adsorption process to ensure that the high efficiency of the process is achieved. According to Buekens and Zyaykina (2001), typical requirements for commercial adsorbents that have been used in adsorption process are:

- High porosity, high internal surface
- High adsorption efficiency in wide range of adsorbate concentration

- Good balance between macro-pores (for fast internal transport) and micro-pores (for large internal surface)
- Hydrophobic chemical structure (for treatment of moist gases) unless the adsorbent is to be used as a desiccant
- Thermal stability unaffected by a cyclic regeneration

There are several types of adsorbents that have been used for adsorption process including activated carbon, zeolite, silica material, activated alumina, and oil palm biomass. The advantages and disadvantages of those adsorbents on Pb(II) removal can be summarized in Table 2.4.

Table 2.4 Advantages and disadvantages of adsorbents

Adsorbent	Advantages	Disadvantages	References
Activated carbon	• Easy to manufacture • highly effective at removing non-polar organic chemical	• Low loading capacities • relatively weak interactions with metallic cations (metal ion binding constants) • Limited to wastewater with low concentration (<5%) • high regeneration cost	(Buekens & Zyaykina, 2001; Lemley et al., 1995; Tavallali & Shiri, 2012)
Zeolites	• High thermal and chemical stability	• size of synthesis molecule is limited • sensitivity to the molecule are low	(Buekens & Zyaykina, 2001)
Mesoporous silica	• Large surface area, chemically inert • thermally stable • biocompatible	• Can dissolve under certain condition • costly	(Buekens & Zyaykina, 2001; Gustafsson et al., 2016)
Activated alumina	• Superior mechanical strength and resistance	• High regeneration heat (205 ºC)	(Buekens & Zyaykina, 2001)
Oil Palm Biomass	• Low cost • exist in abundant	• Low adsorption capacity • increases COD and BOD	(Ahmad et al., 2011)

In brief, activated carbon is the most popular adsorbent for adsorption of Pb(II) process due its effectiveness. However, owing to its advantages as listed in Table 2.4, silica material has been considered as suitable adsorbent for Pb(II) removal owing to its

cost-effectiveness, low regeneration temperature, non-flammable, high mechanical strength, and simple equipment required for process.

2.5 Utilization of Waste Material as Silica Source

Waste material such as fly ash, palm ash, and rice husk ash have attracted significant consideration to be used as alternative silica sources due to the high silica composition. Furthermore, utilization of silica from waste material would minimize the cost of production and reduces the pollution created by the waste material. The subtopic 2.8.1 to 2.8.3 were described in detail the properties of some waste materials.

2.5.1 Fly Ash

Fly ash is a by-product from the combustion of ground or powdered coal and move by flue gasses to the particle removal system from the combustion zone (George, 2018). The combustion of pulverized coal produced about 80-90% of fly ash, while, 10-20% more were dry bottom ash (Abubakar & Baharudin, 2012). The quantity of fly ash produced depends on the quality of coal used and the operating conditions of thermal power plants. The estimated production of coal ash in the world is around 700 million tons and fly ash is 80% of the total ash produced (Argiz et al., 2015). A huge volume of fly ash produced from coal-based thermal power plants may bring several problems from the environmental point of view. Fly ash is hard to manage since it cannot be disposed of (damage to aquatic life), cannot move to another place (particles ranging in size from 1 to 150 μm), and it required a huge land for making ash pond or dikes (Sett, 2017).

Fly ash is considered as ferro-aluminoslicate minerals with major constituents of fly ash are primarily oxides of Si, Al, Fe, Ca, and Mg which constitute about 95-99% of total constituent (Sijakova-ivanova et al., 2011). Minor constituents of fly ash are Ti, Na, K, and S comprises 0.5-3.5% (Szponder & Trybalski, 2011). The physical and chemical composition of fly ash is given in Table 2.5 and Table 2.6, respectively.

Table 2.5 Physical composition of Fly ash

Properties	**Value**
Specific gravity	1.9-2.55
Density (g/cm^3)	1.6-3.2
surface area (cm^2/g)	5.77

Particle size (µm)	1-150
Color	Tan to dark grey

Source: (George, 2018)

Table 2.6 Chemical composition of Fly Ash

Component	**Mass (%)**
Silicon dioxide (SiO_2)	27.88-59.40
Aluminium Oxide (Al_2O_3)	5.23-33.99
Iron oxide (Fe_2O_3)	1.21-29.63
Calcium oxide (CaO)	0.37-27.68
Magnesium Oxide (MgO)	0.42-8.79
Sulfur Trioxide (SO_3)	0.04-4.71
Potassium oxide (K_2O)	0.64-6.68
Titanium Dioxide (TiO_2)	0.24-1.73
Sodium oxide (Na_2O)	0.20-6.90
Other alkaline and unidentified	4.0-6.0
Loss of ignition	0.21-28.37

Source: (Argiz et al., 2015)

The use of fly ash as an alternative silica source for production of mesoporous silica has been proved by the researcher. Yan et al. (2016) reported the use of fly ash for the synthesis of ordered mesoporous nano-silica with 46.62% of silica extracted from the fly ash under alkali-dissolution method with 1.5:1 ratio of sodium hydroxide and solid-liquid solution at 110 °C in 30 min reaction time. Moreover, Dhokte et al. (2011) has reported the synthesis of MCM-41 using fly ash as the silica source. In their study, 60.16% of silica was successfully extracted from the fly ash.

2.5.2 Sugarcane bagasse

Sugarcane bagasse is one of the by-products from agriculture industry. The extraction of juice from sugarcane produced by-products, sugarcane bagasse. Usually, sugarcane bagasse used as a fuel to fire furnace in same industry due to the high amount of un-burnt matter and oxide group (Si, Al, Fe, Ca) in 8-10% yields of ashes, but, sugarcane bagasse directly from industry not effective for fire furnace because of uncontrolled conditions and high temperature of combustion (Goyal et al., 2016). Thus, sugarcane bagasse becomes an industrial waste and poses a disposal problem. About 26% of sugarcane bagasse ash (SCBA) produced by one tonne of sugarcane, whereas, 0.62% contain residual ash (Sundaravadivel & Mohana, 2018).

In SCBA, it contains approximately 50% of cellulose, whereas, another 50% of hemicellulose and lignin (25% each) (Goyal et al., 2016). Table 2.7 andTable 2.8 show the physical and chemical properties in sugarcane bagasse ash respectively.

Table 2.7 Physical properties of sugarcane bagasse ash

Properties	**Value**
Specific gravity	2.68
Density (g/cm^3)	2.52
surface area (cm^2/g)	5140
Particle size (µm)	28.9
Color	Reddish grey

Source: (Goyal et al., 2016)

Table 2.8 Chemical Composition of sugarcane bagasse ash

Component	**Mass (%)**
Silicon dioxide (SiO_2)	62.43
Aluminium Oxide ($Al2_2O_3$)	4.38
Iron oxide (Fe_2O_3)	6.98
Calcium oxide (CaO)	11.8
Magnesium Oxide (MgO)	2.51
Sulfur Trioxide (SO_3)	1.48
Potassium oxide (K_2O)	3.53
Loss of ignition	4.73

Source: (Goyal et al., 2016)

The high content of the silica in SCBA has attracted considerable attention to be used as an alternative silica source in the synthesis of mesoporous silica. Norsuraya et al. (2016) reported the utilization of SCBA as an alternative silica source for synthesis of SBA-15. In their study, 53.10% of silica was successfully extracted from the SCBA. Moreover, Sriatun et al. (2018) reported a preparation of zeolite using silica source from SCBA. A synthesized zeolite has comparable physical and chemical properties with the commercial zeolite, indicating high potential of SCBA as an alternative silica source.

2.5.3 Rice Husk Ash

The production of rice in the world is approximately 580 million per year and keep increasing due to the rising of the world population (Reddy & Marcelina, 2006). The milling of rice has produce rice husk, which is considered as waste material (Patil et al., 2014). An average of 20% rate by weight of the rice husk was produced by rice

during the process (Todkar et al., 2016). Rice husk contains 14-25% of ash which is a unique crop residue with uniform size (Patil et al., 2014). The composition in rice husk is shown in Table 2.9.

Table 2.9 Composition of Rice husk

Element	Percentage (%)
Carbon	37.5
Hydrogen	5.4
Oxygen	36.6
Nitrogen	0.5
Ash	20.0

Source: (Todkar et al., 2016)

In Malaysia, according to the statistics compiled by the Malaysian Ministry of Agriculture, 408,000 tan of rice husk ash produced annually (Daffalla et al., 2012). Amorphous silica will be produced with burning of RHA at temperatures of 550 °C – 800 °C, while crystalline silica will be produced at higher temperatures (Omatola & Onojah, 2009). The particular chemical and physical properties are given in Table 2.10 and Table 2.11, respectively.

Table 2.10 Physical properties RHA

Properties	Value
Specific gravity	2.05
Density (g/cm^3)	1.68
surface area (cm^2/g)	5140
Particle size (µm)	10-45
Color	Black

Source: (Issaraporn & Chareonpanich, 2000)

Table 2.11 Chemical properties RHA

Component	Mass (%)
Silicon dioxide (SiO_2)	94.95
Aluminium Oxide (Al_2O_3)	0.39
Iron oxide (Fe_2O_3)	0.26
Calcium oxide (CaO)	0.54
Sodium oxide (Na2O)	0.25
Potassium oxide (K_2O)	0.94
Manganese(II) Oxide(MnO)	0.16
Titanium(II) Oxide(TiO)	0.02

Magnesium Oxide (MgO)	0.90
Phosphorus pentoxide (P2O5)	0.74
Loss of ignition	0.85

Source: (Patil et al., 2014)

The above composition clearly indicates silicon dioxide, SiO_2 as a major constituent of the rice husk ash. The utilization of RHA as an alternative silica source was reported by Bhagiyalakshmi et al., (2010) in synthesis of chloropropylamine grafted mesopororous MCM-41, MCM-48, and SBA-15 to be applied in CO_2 chemisorption.

2.6 Silica-based Materials

Silica-based material has been studied widely in biological and chemical advanced application such as adsorption, drug delivery, catalysis, and photochemistry due to their high potential towards the organic and inorganic compounds (Javadian et al., 2017; Kushwaha et al., 2017). The interesting chemical and physical properties of material such as high surface area, unique morphology, and the present of Si-O and Si-OH groups on the surface have improved the effectiveness of this material in wide application (Anbia & Hariri, 2010).

2.6.1 Mesoporous Silica

Mesoporous silica has attracted considerable attention due to the wide range of applications such as in catalysis, drug delivery, separation, sensors, photonics, and adsorption. According to the International Union of Pure and Applied Chemists (IUPAC), mesoporous silica are materials with pores in the range of 2–50 nm. The pores of the mesoporous silica have different shapes such as cylindrical or spherical and arranged in varying structures as shown in Figure 2.3.

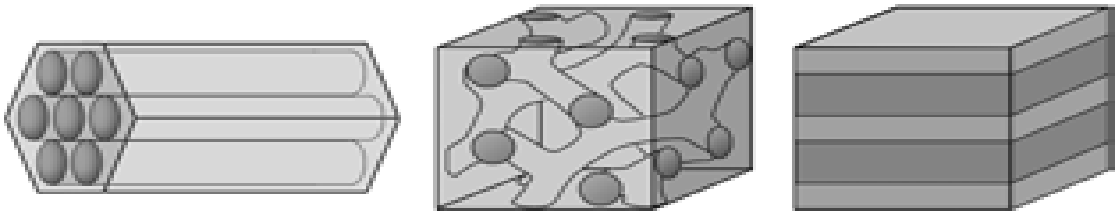

Figure 2.3 Different pore structure of mesoporous material

Unique properties of mesoporous silica have attracted researcher to find new type of family to increase the efficiency of usage. The physical properties such as large surface area, stable, and chemically inert have significant effect on the application performance. Subtopic 2.7.1.1-2.7.1.3 discussed in detail some of the type of mesoporous silica and their applications.

2.6.1.1 Mobil Crystalline of Materials (MCM-41)

The first mesoporous silica is reported in 1992 and this became the starting point of a new research field. This material discovered by Back and co-worker at Mobile Corporation Laboratory and named MCM-X (Mobil Crystalline of Materials) (Vadia & Sadhana, 2011). The structural design of MCM-41 with hexagonal ordered cylindrical pores (MCM-41) synthesized is as illustrated in Figure 2.4.

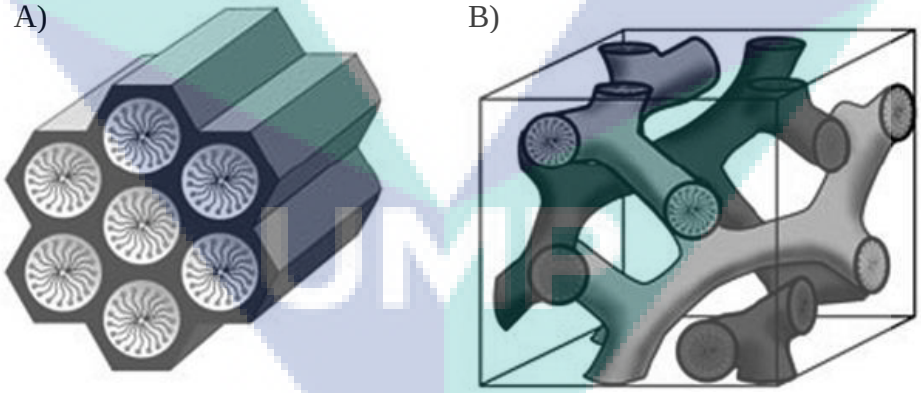

Figure 2.4 Structural design of, (A) MCM-41 and (B) MCM-48
Source: (Alfredsson, 2015)

The silica is synthesized by adding the silica source such as TEOS into the surfactant solution. The CTAB as a micelle was used as the surfactant to give the template of the structure and was removed using calcination process as shown in Figure 2.5.

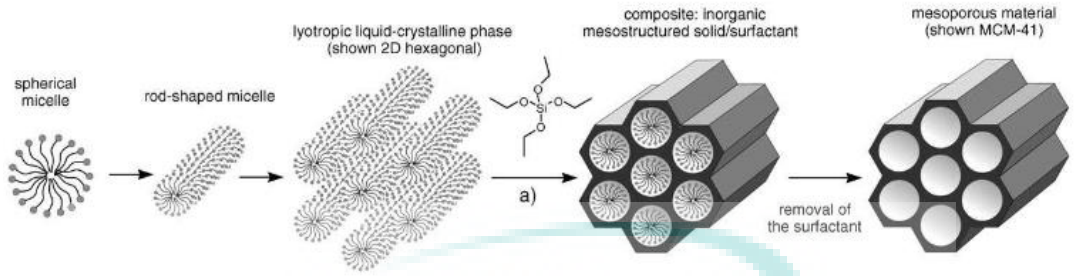

Figure 2.5 Illustrated mechanism of MCM-41

The unique properties of MCM-41 such as large pore volume, high surface area, tunable pore diameter, narrow pore size distribution, easily modified surface, good biocompatibility, and thermal stability (Jhadhav et al., 2015), have attracted considerable attention to be used as adsorbent in adsorption process. Oshima et al. (2006) has reported the used of mesoporous silicate MCM-41 for adsorption of Pb(II) and Cd(II) in benzene from alkaline aqueous solution. From their study, only minimal Cd(II) was removed from aqueous solution, while, the removal of Pb(II) was 80%. Besides, Heidari et al. (2009) studied the removal of Ni(II), Cd(II), and Pb(II) from ternary aqueous solution onto MCM-41, nanoparticle of MCM-41, amino functionalized MCM-41 (NH_2-MCM-41), and nano NH_2-MCM-41. In their study, nano NH_2-MCM-41 (Ni(II) = 92%, Cd(II) = 93% and Pb(II) = 97%) show the higher adsorption capacity followed by NH_2-MCM-41 (Ni(II) = 92%, Cd(II) = 93% and Pb(II) = 95%), nano MCM-41 (Ni(II) = 15%, Cd(II) = 47% and Pb(II) = 75%), and MCM-41 (Ni(II) = 8.2%, Cd(II) = 2.8% and Pb(II) = 29%).

2.6.1.2 Santa Barbara Amorphous (SBA-15)

In 1998, Zhao et al. reported new mesoporous silica with non-ionic triblock polymer with the name SBA-X (Santa Barbara Amorphous) (Zhao et al., 1998). The X in SBA-X is a corresponding number for a specific pore structure and surfactant. SBA-15 is one of the SBA-X family with hexagonally ordered cylindrical pores synthesized with P123 as surfactant (Galameau et al., 2002). The structure of SBA-15 is illustrated in Figure 2.6.

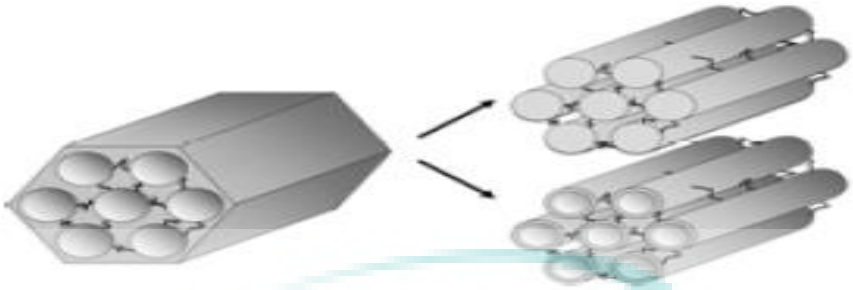

Figure 2.6 The structure of SBA-15
Source: (Thielemann et al., 2011)

SBA-15 has large surface area, uniform-sized pores, thick framework walls, small crystallite size of primary particles, and complementary textural porosity (Huirache-Acuña et al., 2013). The pore sizes in this material refers to the width of the cylindrical pores (Thielemann et al., 2011). To add, the surrounding of each mesopore is the microporous network called corona which occurred (Diao et al., 2010) that interconnects the mesopores with each other and is responsible for the high surface area of SBA-15. The corona is mainly supposed to originate from trapped hydrophilic chains of the surfactants (Alfredsson, 2015).

The use of SBA-15 has been reported by numerous researches including Li et al. in the study of amino-functionalized fly-ash-based SBA-15 in adsorption of Pb(II) (Li et al., 2017) and Hernández-Morales et al. in the study of SBA-15 functionalized with -NH_2 for adsorption of Pb(II) (Hernández-Morales et al., 2012). From their studies, 98% and 93% of Pb(II), respectively, was successful being removed from the aqueous solution.

2.6.1.3 Mesoporous Silica Nanoparticles (MSN)

Mesoporous Silica Nanoparticles (MSN) was first introduced in 2015 by Paul J. Kempen and co-worker (Kempen et al., 2015) for drug delivery due to the lack availability of contrast agent in present mesoporous silica. The synthesis MSN was reported using sol-gel method with TEOS as silica sources. The general structure of MSN is shown in Figure 2.7.

Figure 2.7 The structure of MSN

Sources: (Quan et al., 2015)

MSN promising interesting characteristic is equivalent with another silica-based material which is tunable pore diameter and size, high pore volume, excellent biocompatibility, high loading ability, large surface area, and can be functionalized due to its topologically distinct domain (Jadhav et al., 2015; Jafari et al., 2019; Kempen et al., 2015). To improve the effectiveness of nanocarriers, surface modification has been widely studied using molecules such as arginine-glycine-aspartic (RGD) (Niu et al., 2018), amine group (Naowanon et al., 2018), folate (Fan et al., 2016), carboxymethyl chitosan (CMCS) (Xu et al., 2018), and lactose (Quan et al., 2015).

The MSN has been widely used in medical application such as drug delivery (Jadhav et al., 2015), DNA loading (Niu et al., 2018), therapeutic or diagnostic (Jafari et al., 2018), gene delivery (Fan et al., 2016), and improved anticancer efficiency (Pan et al., 2017). Besides, MSN has been used in heavy metal adsorption as reported by Naowanon et al., (2018) for removal of Cu^{2+} and Fe^{2+} from aqueous solution. They found around 99% of Cu^{2+} and 95% of Fe^{2+} were successfully removed from aqueous solution using MSN as adsorbent.

2.6.2 Fibrous Silica Nanosphere (KCC-1)

KCC-1 is the first nanoparticle developed by King Abdullah Universiti of Science and Technology (KAUST) Catalysis Center, in the year 2010 (Le et al., 2014). KCC-1 also known as Fibrous Silica Nanosphere. KCC-1 offers a unique alternative shape, other than porous that has never been seen in silica materials which is a fibrous surface

morphology arranged in a three-dimensional structure to form spheres (Figure 2.8) (Dong et al., 2015).

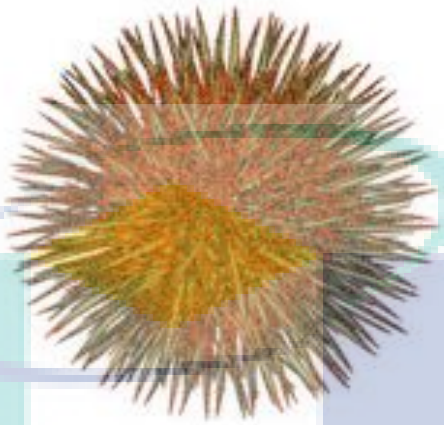

Figure 2.8 KCC-1 strucure
Source: (Dong et al., 2015)

Unlike traditional pore-based silica, these nanospheres possess a fibrous structure that dramatically increases the accessibility to most of the available surface area. This, in turn, increase the adsorption capacities and the removal percentage significantly. Test performance on the KCC-1 also offered better performance than other silica-based system like SBA-15 and MCM-14 in various applications related to catalysis and sorption (Qureshi et al., 2016). Table 2.12 described some characteristics of KCC-1.

Table 2.12 Characteristics of KCC-1

Properties	Value
Average particle size	200-400 nm (Other particle sizes can be synthesis)
Surface area	>386 m^2/g
Mechanical stability	Up to 216 MPa
Polydispersity index (PDI)	0.2-0.25
Bulk and tapped density	0.18-0.19 and 0.2 g/cm3
Viscosity	0.0005 Pas at 25 ºC (5% solution)
Thermal stability	Up to 800 ºC

Source: (Basset et al., 2010)

KCC-1 has been reported in numerous applications such as catalysis, photocatalysis, CO_2 capture-conversion, sensing, detection and extraction of ions, supercapacitors, drug deliveries, and other biomedical applications. Fihri et al., (2012) reported that high surface area of KCC-1 with dendrimeric morphology had triggered

towards better Ru particles dispersion and led towards superior hydrogenolysis process with no deactivation up to eight days of the reaction. Besides, Huang et al., (2014) mentioned that a higher adsorption capacity of salmon DNA over KCC-1 based nanomaterials as compared to MCM-41 based nanomaterials due to the large pores, wide pore mouths, fibrous pore network and high accessibility with an amenable structure of the catalyst. An excellent catalytic performance was also possessed by KCC-1 towards CO_2 methanation whereby it produced 38.9% of CH_4 which was five-fold higher than MCM-41 due to spherical morphology with larger particle size of dendritic fiber (200-400 nm) and higher surface area (773 m^2/g) (Hamid et al., 2017). In addition, KCC-1 also has a good performance in CO_2 capture with a total 91.5 mmol/g CO_2 capture volume, which is higher than that of MCM-41 (73.1 mmol/g) on account of its extraordinary fibrous morphology (Singh & Polshettiwar, 2016). However, no study was reported on the application of KCC-1 in the adsorption process. Thus, in this study, KCC-1 was used in the adsorption process.

KCC-1 was commonly synthesized using an expensive silica source which is tetraethyl orthosilicate (TEOS), thus efforts can be made to use inexpensive sodium silicate as a silica source. The use of extracted sodium silicate prepared from waste material in the synthesis of mesoporous silica was promising as reported by other researchers in the synthesis of other mesoporous silica such as SBA-15 and MCM-41. Wang et al., (2016) reported the utilization of coal gangue as alternative silica source in the synthesis of SBA-15. In their study, 95.21% of silica was successfully prepared from coal gangue and was used in synthesis of SBA-15 (S-slag). The characterization results showed that the properties of SBA-15 synthesized from coal gangue was comparable with SBA-15 synthesized from commercial sodium silicate (S-100), indicating the high potential of waste as an alternative silica source for preparation of silica-based material. Thus, in this study, waste material (rice husk ash (RHA)) will be utilized for preparation of sodium silica and will be used as the silica source in KCC-1 synthesis.

2.7 Optimization study

Optimization is an important step in adsorption study because it will determine the best condition for the maximum removal. Response surface methodology (RSM) is one of the optimization methods and was discovered in 1950s by Box and Wilson (Mäkelä, 2017). It basically a collection of mathematical and statistical methods that is

useful for designing the experiments, developing models by considering the interactions of parameters, and process optimization. In simple word, RSM is the optimization of the response using specific set of the experiment with a different condition for each set. This technique was widely used in chemical reaction that involving more than one response (Setiabudi et al., 2013).

Response surface methodology (RSM) technique has attracted researchers' attention owing to its advantages as compared to the conventional experimental technique which is one-variable-at-a-time technique. Table 2.13 listed in detail the differences between RSM and one-variable-at-a-time technique.

Table 2.13 Differences between response surface methodology (RSM) and one-variable-at-a-time technique

Response surface methodology (RSM)	**One-variable-at-a-time**
Each run of the experiment has different range of the variables	Each experiment only changes one variable while other constant
Each of the studied variables was interact with each other in different run of the experiment.	Lack of the interaction between the study variables
Economical due to the small number of the experiment	Not economical due to greater number of the experiments, thus increasing time, expenses, reagent and material.

Sources: (Bezerra et al., 2008; Wani et al., 2012; Zolgharnein et al., 2013)

From the table above, it can be concluded that the RSM has advantages in the optimization as compared to the conventional experimental technique (one-variable-at-a-time). In addition, RSM technique is more convenient in optimization process due to the different range variables interaction occurred in each set of runs, thus, more specific optimum condition with high adsorption capacity can be achieved.

2.7.1 Theory and steps for RSM application

Response surface methodology (RSM) was sequentially applied until the optimum or near optimum condition reached. The relationship between response of the process, Y, and the input factors can be described using equation (2.1):

$$Y = f(X_1, X_2, X_3, ..., X_n) + \varepsilon \quad (2.1)$$

Where Y is a response of the process, f is the real response function and its format being unknown, X_1, X_2, X_3, ..., X_n is an input variables with n is a number of input variables, and ε is the residual error.

Several steps in application of RSM as modelling and optimization technique as follows; (1) screening and performing a series of design experiment; (2) running the experiment and fitting the obtained mathematical model to experimental data; and (3) determination of optimum condition (Sadhukhan et al., 2016). Subtopic 2.10.1.1 to 2.10.1.3 explained in detail about these steps.

2.7.1.1 Screening and performing a series of experimental design

Before the optimization using RSM started, the independent variables that affect the process must be screened. The screening process can be done by conducting preliminary screening experiment or literature review. The factor that affecting the process was listed, and from the listed factor, variables that give a significant effect in the process and independent of each other were chosen. Besides, the ranges for these variables must also be chosen from reasonable sources to prevent unreliable and uninformative results for the final outcomes. In general, the variables values are coded to compare their effect within the design range and shown in equation (2.2):

$$X_i = \frac{(X_1 - X_{\min})}{\Delta X / 2} - 1 \qquad (2.2)$$

where X_i is a coded value, X_1, X_{min} and ΔX is a variable value, minimum variable value and variable range, respectively, in original unit.

After the screening process, the experiment was designed by selecting the points where the responses must be estimated and evaluated. The selection of the suitable experimental design is important to get an accuracy on the prediction of the optimum condition (Sakkas et al., 2010). Central composited design (CCD) and Box-behnken (BB) were the main types of experimental design. The CCD would determine both linear and quadratic models and the number of run experiment would be determined by using equation $N=k^2+2k+C_p$; where k is the variable number and C_p is a replication number of the central point, whereas, BB was a three-level factorial arrangement with the number of experimental run was determined by $N=2k(k-1)+C_p$; where k is the variable number and C_p is a replication number of the central point (Bezerra et al., 2008; Ferreira et al., 2007; Zolgharnein et al., 2013). Even though, the number of experimental run for CCD

was higher as compared to the BB, however CCD was commonly used since the efficiency of BB was very low for higher number of variables (Bezerra et al., 2008). Several computer software can be used for this method such as Design Expect (State-Ease Inc), Minitab (Minitab Inc.) and Statistica (Stat Soft).

2.7.1.2 Running the experiment and fitting the obtained mathematical model to experimental data

After choosing the design of the experiment, the experiment was done using a set of experiment with a certain order generated from computer software. The obtained result was assumed as response in the software and analyses using mathematical model.

The mathematical model must be fitted to the experimental result to validate the whole procedures. RSM should sequentially fit the first-order model to second-order model due it mainly base on second order model. The second-order model can be described as follows:

$$Y = \beta_0 + \sum \beta_i X_i + \sum \beta_{ii} X_i^2 + \sum \beta_{ij} X_i X_j \quad (2.3)$$

The application of analysis of variance (ANOVA) used to evaluate the quality of the fitted model using *F-value*. *F-value* can be calculated using equation (2.4):

$$F - value = \frac{MS_{SSR}}{MS_{SSE}} \quad (2.4)$$

where MS_{SSR} is a mean of square regression and MS_{SSE} is a mean of square residual. The calculated *F-value* should be higher than tabulated *F-value* to reject null hypothesis. The significant of the model can be described by *t-value* and *p-value*.

2.7.1.3 Determination of optimum condition

The optimal condition of the study can be described by the surface generated by linear model. In this study, the surface can be visualized using the surface response plot. The surface response plot represents three-dimensional plot with three axes represent 2 variables and 1 response. However, if variables are three or more, the one or more variables must set to a constant value. Figure 2.9 shows some of the quadratic responses surface plot profile with optimization of two variables. Figure 2.9(a) and Figure 2.9(b) surfaces show the maximum point was located inside the experiment region, with no

changes detected on variable X_2 in Figure 2.9(b), indicating that these variables do not affect the studied system. Figure 2.9(c) shows that the maximum point was outside the experimental region and Figure 2.9(d) represents a minimum point. The surface of Figure 2.9 (e) shows the critical point presents by saddle point. The saddle point was an inflexion point between a relative maximum or minimum response to a studied system, the saddle point coordinates do not serve as optimal values (Bezerra et al., 2008).

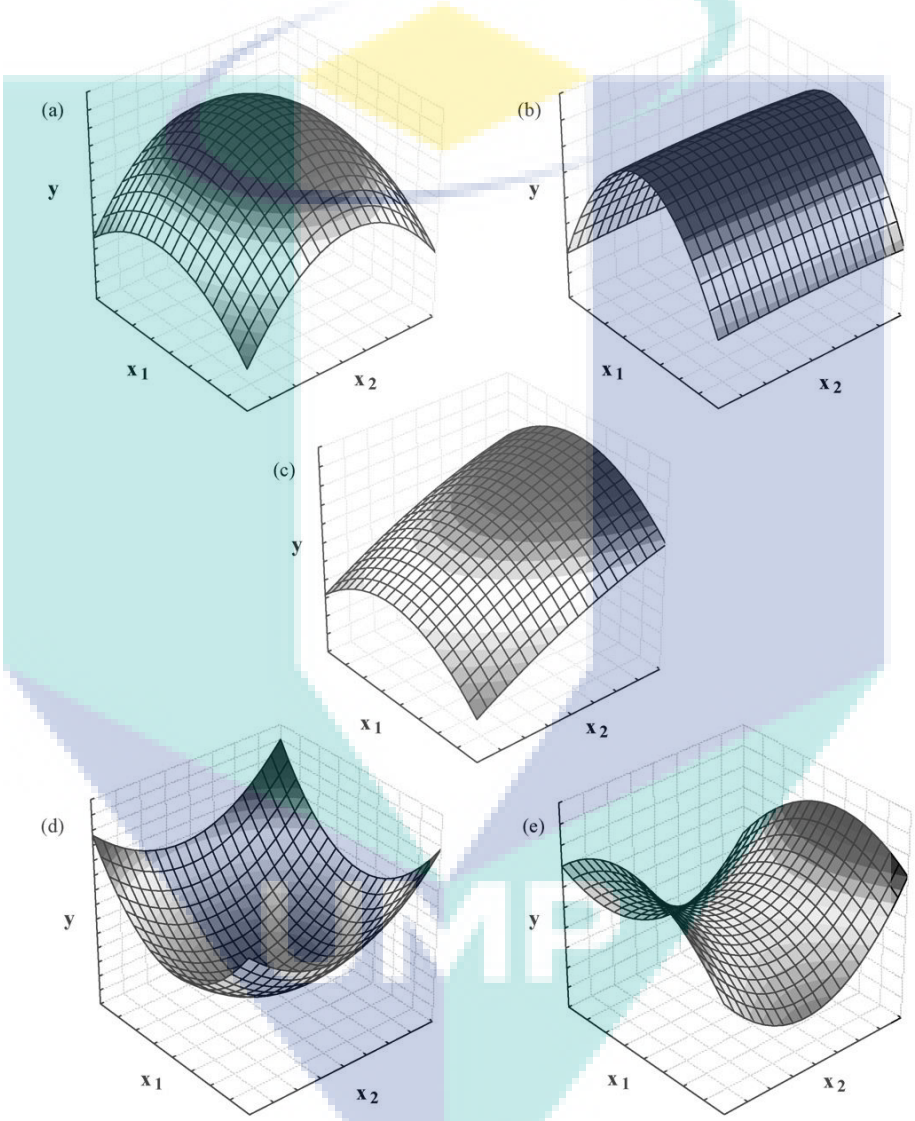

Figure 2.9 Quadratic response surface plot profile
Source: (Bezerra et al., 2008)

2.7.2 Application of Response Surface Methodology

Response surface methodology (RSM) was widely used in various application such as food research (Madamba, 2002; Marcin et al., 2016; Nazni & Gracia, 2014; Yolmeh & Jafari, 2017), photocatalytic (Keramati et al., 2016; Khataeea et al., 2011; Sharma et al., 2015), and adsorption (Ardekani et al., 2017; Azad et al., 2016; Kalantari et al., 2014; Latchubugata et al., 2018). Various application of RSM was reported in adsorption study due to the great advantages of RSM such as reducing the number of experimental required to evaluate the various parameter and their interaction.

Ahmad and Hasan (2016) has reported the use of RSM in optimization of Pb(II) removal from aqueous solution onto PAB nanocomposite. In this study, they optimized five variables (agitation time, pH, dose, initial concentration and temperature) with 52 sets of the experiment. The optimum conditions were achieved at agitation time of 172 min, pH of 4.0, dose of 0.06 g, initial concentration of Pb(II) of 55 mg/L and temperature of 44 °C, with Pb(II) removal of 96.65% and regression coefficient (R^2) of 0.99. Kahkha et al. (2014) also explored the application of RSM with central composite design (CCD) for Pb(II) from aqueous solution using Prosopis Stephanian Fruits. A set of 20 runs was executed to analyse the adsorption process and the optimum conditions were achieved at 4.60 g/L of adsorbent dosage, 4.0 of pH, and 37.5 mg/L of initial Pb(II) concentration, with 98% of removal. The successful reported literatures on the optimization of Pb(II) removal onto adsorbent revealed the efficiency of RSM in optimization process.

2.8 Summary

In summary, Lead (Pb(II)) has been chosen as an adsorbate owing to its toxicity even at low concentration and non-biodegradable. The exposer of the Pb(II) to the body through inhalation and ingestion of food or water will cause serious diseases and permanent damage to human health. Besides, World Health Organization (WHO) also stated that only less than 0.01 mg/L concentration of Pb(II) is allowable in drinking water (World Health Organization, 1984). Thus, owing to the high toxicity of Pb(II), concentration of Pb(II) must be reduced before discharge to the surrounding using suitable removal technique. In this study, adsorption method has been chosen as the removal method owing to its economical, simple and flexible of design (Al-Rashdi et al.,

2011; Fu & Wang, 2011; Kalantari et al., 2014; Vijayalakshmi et al., 2017). Besides, this process also produces minimum biological and chemical sludge.

Regarding the selection of adsorbent, fibrous silica nanosphere (KCC-1) has attracted considerable attention owing to its high surface area and fibrous silica morphology. However, owing to the high cost of commercial silica precursor, the utilization of waste material as alternative silica source seems to be a promising approach and the application of amine functionalization will enhance its adsorption capacity. According to literatures, several waste materials containing high amount of silica are summarized in Table 2.14.

Table 2.14 Summary for properties alternative silica source

Properties	**Fly Ash**	**Sugarcane Bagasse Ash (SCBA)**	**Rice Husk Ash (RHA)**
Specific gravity	1.9-2.55	2.68	2.05
Density (g/cm^3)	1.6-3.2	2.52	1.68
surface area (cm^2/g)	5.77	5140	5140
Particle size (µm)	1-150	28.9	10-45
Color	Tan to dark gray	Redish grey	Black
SiO_2 (%)	27.88-59.40	62.43	94.95
Al_2O_3 (%)	5.23-33.99	4.38	0.39
Fe_2O_3 (%)	1.21-29.63	6.98	0.26
CaO (%)	0.37-27.68	11.8	0.54
MgO (%)	0.42-8.79	2.51	0.90
K_2O (%)	0.64-6.68	3.53	0.94
LOI (%)	4.69-47.71	6.21	2.02

From the Table 2.14, it is clearly showed that rice husk ash (RHA) contains higher silica dioxide (SiO_2) as compared to fly ash and sugarcane bagasse ash (SCBA). Thus, RHA was used as an alternative silica source for synthesizing of KCC-1 and thus was applied as adsorbent in Pb(II) removal.

CHAPTER 3

METHODOLOGY

3.1 Material

Table 3.1 shows all materials used in this study. The high purity materials were used in this study to ensure the effectiveness of the result.

Table 3.1 List of material used

Materials	Purity	Brand/Company
Rice husk ash (RHA)	-	LLH Biomass Sdn. Bhd, Alor Setar, Kedah
Hydrochloric acid (HCl)	37%	Merck
Sodium hydroxide (NaOH)	97%	Merck
Cetyltriammonium bromide (CTAB)	≥ 98%	Sigma
Urea	≥ 99.5%,	Merck
1-Butanol	≥ 99.5 %	Merck
Toluene	-	Merck
Lead Nitrate ($Pb(NO_3)_2$)	≥99%	Sigma
Dithizone	-	Merck

3.2 Preparation of adsorbent

3.2.1 Extraction of sodium silicate from RHA (Na_2SiO_3-RHA)

The RHA was washed thoroughly with water to remove adhering dust and soil, and then dried at 120 °C overnight. Then, RHA was calcined at 600 ºC for 6h to remove organic impurities in RHA. Acid-soluble elements was removed by acid leaching whereby the calcined RHA and 100 mL of 2 M HCl solution was stirred at 60 °C for 3 h. The mixture was filtered and the solid residue was dried at 120 °C overnight followed by calcination at 550 °C for 3 h. X-ray Fluorescence Spectrophotometry (XRF, Bruker S8 TIGER ECO) analysis of RHA and acid leaching-RHA (ARHA) were performed to verify the composition of the RHA and ARHA. The result revealed that SiO_2 is the major

constituent of RHA (88.52%) and ARHA (95.44%), indicating that RHA is an alternative low-cost material for commercial sodium silicate (Na_2SiO_3) and pretreatment of RHA with HCl is required to improve the purity of SiO_2 in RHA.

The solution of Na_2SiO_3-RHA was prepared using alkali fusion method whereby specific amount of RHA will be mixed with sodium hydroxide powder (NaOH, Merck) and was calcined at 550 ºC for 1 hour to form NaOH-fused RHA. The NaOH-fused RHA then was cooled to room temperature and crushed to obtain a powder form of NaOH-fused RHA. The obtain powder was mixed with deionized water followed by stirring for 24 h. Then, the solution was filtered to collect the supernatant known as Na_2SiO_3-RHA. Silica content in Na_2SiO_3-RHA was 6%, revealed by the Couple Plasma Mass Spectroscopy (ICP-MS).

3.2.2 Preparation of KCC-1

The method for preparation of KCC-1 was described by Dong et al. (Dong et al., 2014). In brief, the experimental started with stirring the specific amount of Na_2SiO_3-RHA, 1.5 mL of butanol (Merck) and 30 mL of toluene (Merck) in one beaker, whereas the stirring of 0.6 g urea solution of (Merck), 1 g of cetyltriammonium bromide (CTAB, Aldrich), and 30 mL of water was placed in another beaker. Then, both solutions were fused and stirred at ambient temperature for 45 min before heated for 5 h at 120 ºC in a Teflon-sealed hydrothermal reactor. The solution obtained was centrifuged, rinsed using distilled water and followed by oven-dried at 100 ºC overnight. The sample was calcined at 550 ºC in air for 5 h and KCC-1(RHA) was acquired. The commercial KCC-1 was also synthesized using commercial sodium silicate (Na_2SiO_3-C, silica content = 25.5%, Merck) by following the similar procedures, and the sample was designated as SBA-15(C). The silica content during the KCC-1 synthesis using both silica source was fixed at 25.5%.

3.2.3 Characterization of synthesized KCC-1

The crystallinity texture of synthesized KCC-1 was examined via X-ray diffraction (XRD) recorded using powder diffractometer (Miniflex II, Rigaku; 30 kV, 15 mA) within the range of $2\theta = 0°$- 80° with a Cu Kα radiation ($\lambda = 1.54Å$). The functional groups of the synthesized KCC-1 were determined using Fourier-transform infrared spectrometer (FTIR Spectrometer Nicolet iS5, Thermo Scientific). The morphology of KCC-1 was determined via Transmission Electron Microscopy (TEM Leo Libra-120).

Ethanol was used to disperse the sample by sonication before deposited the sample on an amorphous, porous carbon grid. The analysis of the textural properties of KCC-1 was carried out using Bruneuer-Emmett-Teller (BET) (Micromeritics®) at 77 K. By scanning within the range of 4000 – 500 cm^{-1}, the Fourier-Transform Infrared (FTIR Spectrometer Nicolet iS5, Thermo Scientific) analysis was executed to determine the functional group of KCC-1 participated in the removal of Pb(II) process.

3.3 Batch Adsorption

The stock solution (1000 mg/L) was prepared for the adsorption experiment, whereby the accurate amount of Pb(II) nitrate ($Pb(NO_3)_2$, Sigma-Aldich) was dissolved in deionized water to prepare the stock solution. Then, the dilution of the stock solution was done with deionized water to desired concentration (50 – 400 mg/L), before specific amount of KCC-1 (0.5 – 5 g/L) being added to 200 mL of Pb(II) solution under constant stirring at room temperature. According to the result observed on the effect of pH (not shown), the optimum pH was determined to be at pH 6, therefore, the pH of the Pb(II) solution for all the batch adsorption experiments was fixed at pH 6. Moreover, the trend observed could be described on the basis of zero point charge (pH_{zpc}) of KCC-1(RHA), which confirmed to be at ~pH5.8. The samples were collected at the specific time (0 – 140 min) and then centrifuged at 3000 rpm for 2 minutes. The Pb(II) concentration after the batch adsorption were measured using UV-vis spectroscopy at 520 nm. Dithizone was used as a reagent to give brick red colour to the solution.

The values of Pb(II) removed (%) and Pb(II) adsorbed (mg/g) were determined using following equation:

$$\text{Removal}\,(\%) = \left(\frac{C_o - C_t}{C_o}\right) \times 100 \tag{3.1}$$

$$q_t = \left(\frac{C_o - C_t}{m}\right) \times V \tag{3.2}$$

where C_o and C_t (mg/L) is the initial concentration and the liquid-phase concentration of Pb(II) solution at any time, respectively. Moreover, q_t (mg/g) is the value of Pb(II) adsorbed at any time, m(g) is the adsorbent dosage and V (L) is the volume of the Pb(II) solution.

3.4 Experimental design and optimization

In this study, Statsoft Statistica 8.0 software was used for response surface methodology (RSM) analysis equipped with face-centered central design (FCCCD). RSM analysis enables the prediction of the optimal process condition and provides analytical results on the interaction of related process variables. In this process, three main steps were involved which were experimental design, modelling and optimization. Initial concentration, X_1 (50 – 400 mg/L), adsorbent dosage, X_2 (0.5 – 5.0 g/L) and time, X_3 (60 – 180 min) were selected as the independent variables and -1 and +1 was used as a coded for low and high levels, respectively. In this experiment, 16 total number of experiments were conducted including 2^3 factorial points, 6 axial points, and 1 replicate at the middle point. The relationship between response and independent variables was estimated by the following equation:

$$Y = \beta_0 + \beta_1 X_1 + \beta_2 X_2 + \beta_3 X_3 + \beta_{12} X_1 X_2 + \beta_{13} X_1 X_3 + \beta_{23} X_2 X_3 + \beta_{11} X_1^2 + \beta_{22} X_2^2 + \beta_{33} X_3^2 \quad (3.3)$$

Where Y is the predicted response while X_1, X_2 and X_3 are coded form of independent variables. The term β_0 is the offset term; β_1, β_2, and β_3 are the linear terms; β_{11}, β_{22}, and β_{33} are the quadratic terms; and β_{12}, β_{13}, and β_{23} are the interaction term. The variance (ANOVA) analysis was used to appraise the equation model using 5% significant level, whereby the null hypothesis can be eliminated if tabulated F-value lower than calculated F-value. The calculated F-value was determined by referring to the procedure reported in literature (Setiabudi et al., 2013) .

CHAPTER 4

RESULTS AND DISCUSSION

4.1 Characterization of KCC-1

The properties of synthesized KCC-1 were characterized using XRD, FTIR, TEM and BET, and were compared with KCC-1(C). Figure 4.1 shows the XRD pattern of the synthesized KCC-1. The peak centered at $2\theta \approx 23^{o}$ representing the presence of amorphous silica phase in the catalysts (Dong et al., 2014). No significant changes were observed in the XRD pattern, indicating that KCC-1 was successfully synthesized using Na_2SiO_3-RHA.

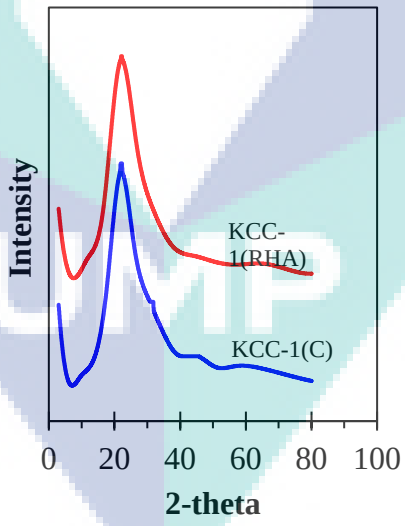

Figure 4.1 XRD pattern of KCC-1(RHA) and KCC-1(C)

The FTIR spectra of the synthesized KCC-1 are shown in Figure 4.2 The peaks at 3425 cm^{-1}, 1055 cm^{-1}, 797 cm^{-1}, and 440 cm^{-1} are attributed to the O-H stretching vibration of Si-OH, symmetrical stretching of Si-O, unsymmetrical stretching of Si-O, and Si-O bending, respectively (Ekka et al., 2015). The intensity of the peaks for KCC-

1(RHA) slightly lower than that of KCC-1(C), indicating the less ordering of silica framework in KCC-1(RHA). Dong et al. (Dong et al., 2015) on the study of KCC-1 modified silver nanoparticles (Ag NPs) (Dong et al., 2014) and Ni@Pd core-shell nanoparticles (Ni@Pd NPs) also reported the existent of amorphous silica phase on XRD peak (2θ =15° - 30°C) and O-H stretching vibration of Si-OH, symmetrical stretching of Si-O, unsymmetrical stretching of Si-O and Si-O bending on FTIR pattern (3200-3500, 1095, 802 and 450 cm^{-1}, respectively), which comparable with the present study.

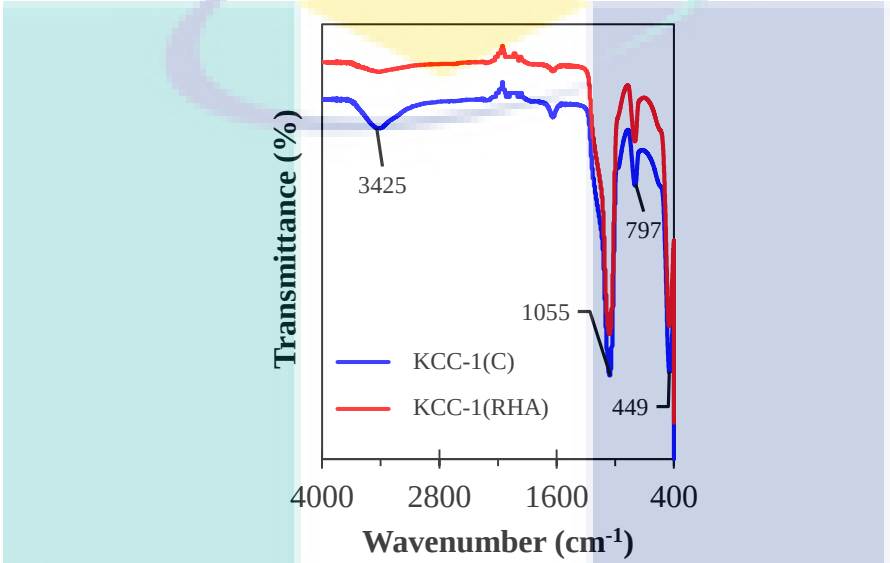

Figure 4.2 FTIR spectra of KCC-1(RHA) and KCC-1(C)

The morphology of KCC-1(C) and KCC-1(RHA) obtained via TEM was illustrated in Figure 4.3. As can be observed, KCC-1(C) are made up of uniform spheres with fibrous morphology. The utilization of Na_2SiO_3-RHA as silica precursor successfully synthesised KCC-1(RHA) with comparable morphology as KCC-1(C).

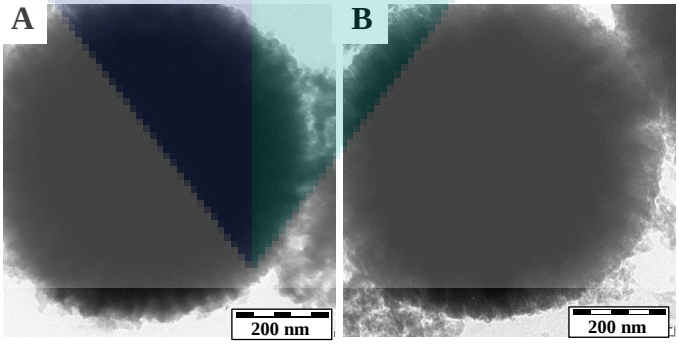

Figure 4.3 TEM image of (A) KCC-1(C) and (B) KCC-1(RHA)

The BET surface area, pore volume and pore size of KCC-1(C) were 227 m^2/g, 1.24 cm^3/g and 21.91 nm, meanwhile, the results for KCC-1(RHA) were 220 m^2/g, 0.94

cm^3/g and 17.37 nm, which slightly lower than that of KCC-1(C). A small difference in the properties of KCC-1(RHA) as compared to the KCC-1(C) might be related with the higher purity of the commercial Na_2SiO_3 as compared to Na_2SiO_3-RHA. This study was in agreement with Rahman et al. (2016) on synthesis of mesoporous silica MCM-41 and SBA-15 from power plant bottom ash as silica sources (BA MCM-41 and BA SBA-15) as comparison with TEOS as silica source (PMCM-41 and PSBA-15). From their study, PMCM-41 (S_{BET} = 561.39 m^2/g and V_p = 0.406 cm^3/g) and PSBA-15 (S_{BET} = 509.41 m^2/g and V_p = 0.497 cm^3/g) has higher BET surface area (S_{BET}) and pore volume (V_p) as compared to the BA MCM-41 (S_{BET} = 5.25 m^2/g and V_p = 0.00477 cm^3/g) and BA SBA-15 (S_{BET} = 71.40 m^2/g and V_p = 0.204 cm^3/g).

4.2 Optimization of Pb(II) removal onto KCC-1(RHA) by Response Surface Methodology (RSM)

The 16 experimental design and corresponding results of response (percentage removal of Pb(II)) are shown in Table 4.1.

Table 4.1 Experimental design and results obtained for Pb(II) removal onto KCC-1(RHA).

Run	Manipulated Variables						Response
	Initial Concentration (mg/L), X_1		Adsorbent Dosage (g/L), X_3		Time (min), X_2		Pb(II) Removal (%), Y
	Uncoded	Coded	Uncoded	Coded	Uncoded	Coded	
1	50	-1	0.5	-1	60	-1	61.00
2	50	-1	0.5	-1	180	1	61.29
3	50	-1	5	1	60	-1	58.87
4	50	-1	5	1	180	1	60.13
5	400	1	0.5	-1	60	-1	69.47
6	400	1	0.5	-1	180	1	69.73
7	400	1	5	1	60	-1	67.69
8	400	1	5	1	180	1	65.83
9	50	-1	2.75	0	120	0	65.70
10	400	1	2.75	0	120	0	72.75
11	225	0	0.5	-1	120	0	69.66
12	225	0	5	1	120	0	69.10
13	225	0	2.75	0	60	-1	70.64
14	225	0	2.75	0	180	1	70.22
15(C)	225	0	2.75	0	120	0	74.59
16(C)	225	0	2.75	0	120	0	74.45

The full quadratic model to represent Pb(II) withdrawal from the aqueous solution onto KCC-1 using RSM analysis is given as the Equation (2).

$$Y = -18.8465 + 0.3102X_1 + 0.2469X_2 + 26.7658X_3 - 0.0004X_1^2 + 0.0008X_2^2 - 2.6263X_3^2 - 0.0007X_1X_2 - 0.0125X_1X_3 - 0.0460X_2X_3 \quad (4.1)$$

where X_1, X_2, and X_3 are the independent variables coded form, whilst, Y is the estimated response.

The statistical significance of the model applied was examined using variance analysis, ANOVA (Asfaram et al., 2015). Total variation was divided into set of the data by ANOVA statistical tool into component parts related with particular variation sources for the sake of examining the model parameter's hypothesis (Ravikumar et al., 2007). By referring to the ANOVA statistical analysis shown in Table 4.2, the model was relatively significant owing to the higher calculated *F*-value (F_{model} = 32.21) than that of the tabulated *F*-value (F_{table} = 4.10) with the respective degree of freedom and probability (p = 0.05).

Table 4.2 ANOVA analysis of Pb(II) removal onto KCC-1(RHA).

Sources	Sum of square (SS)	Degree of freedom (*d.f*)	Mean Square (*MS*)	*F*-value
Regression (SSR)	368.21	9	40.91	32.21
Residual	7.59	6	1.27	
Total (SST)	375.80	15		

The relationship amidst experimental and predicted values were evaluated by plotting the parity plot of predicted and observed values whereby the predicted values were calculated from the regression model whereas observed values observed from the experiments. In brief, the regression coefficient, R^2 of the parity plot must be closed to 1.0 and should be at least 0.8 or greater for a good correlation of a model (Asfaram et al., 2015). High coefficient value of R^2 (0.9798) obtained from the parity plot indicated that the regression model described most of the data variation and thus verified the correlation between the model and the experimental data.

The *p*-value and *t*-value of the independent variables for the Pb(II) removal from aqueous solution onto KCC-1 are shown in Figure 4.4. The *p*-value was used to examine the significance of the coefficient, while, the *t*-value stands for the standard deviation of predictable parameter and proportion of the predictable parameter effect, where

predictable parameter of the regression coefficient value was twice. The significance of the corresponding parameter in regression model was determined by the magnitude of *p*-value and *t*-value. The corresponding parameter with a greater *t*-value magnitude or/and with a smaller *p*-value contributes more significance over the regression model (Setiabudi et al., 2013). As demonstrated in Figure 4.4, the linear term of initial concentration (X_1) (*p*-value = 0.00004, *t*-value = 0.84), quadratic term of initial concentration (X_1^2) (*p*-value = 0.00221, *t*-value = -5.11), quadratic term of adsorbent dosage (X_2^2) (*p*-value = 0.00277, *t*-value = -4.88), quadratic term of time (X_3^2) (*p*-value = 0.01510, *t*-value = -3.37), and linear term of adsorbent dosage (X_2) (*p*-value = 0.03684, *t*-value = -2.67) were statistically significant in this regression due to the large *t*-value magnitude and small *p*-value ($p < 0.05$). The rest of the variable's terms were considered less significant, due to a greater *p*-value ($p > 0.05$). The initial concentration (X_1) was found to be more prominent variable that highly influenced the Pb(II) adsorption onto KCC-1. From the Pareto chart, it can be summarized that the most significant parameter for the regression model was the linear term of initial concentration (X_1), while the linear term of time (X_3) was the least significant factor for the Pb(II) removal onto KCC-1(RHA).

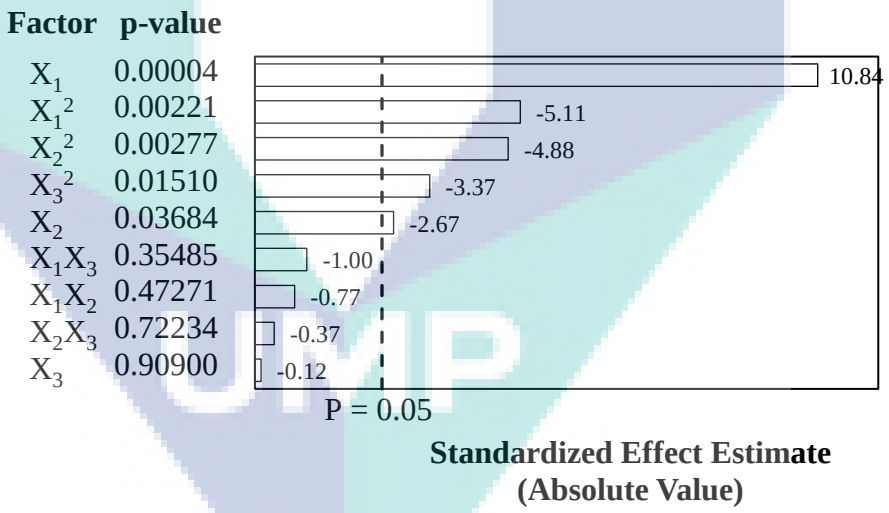

Figure 4.4 Pareto chart and *p*-value for Pb(II) removal onto KCC-1(RHA).

The 3D response surfaces and contours plots between three independent variables were constructed for Pb(II) removal onto KCC-1(RHA) (Figure 4.5), by plotting the graphs with the consideration of two independent variables while the other variable was maintained unchanged at its mean level. Figure 4.5(A) shows the effects of the initial concentration (X_1) and adsorbent dosage (X_2) towards the Pb(II) removal percentage.

From the plot, the increasing of initial concentration (from 50 to 375 mg/L) and adsorbent dosage (from 0.5 to 3 g/L), increased (54-75 %) the Pb(II) removal until the optimum condition (X_1 = 250 – 375 mg/L, X_2 = 1.5 – 3 g/L) was achieved with Pb(II) removal of 74-75%, and decreased at higher values. In brief, the increasing of initial concentration leads to an increase in critical driving forces of Pb(II) ions onto the active sites of the KCC-1 and thus enhance the percentage removal. However, a decrement in removal percentage upon further increasing in Pb(II) ions was related to the Pb(II) ions saturation at limited concentration (Kalantari et al., 2014). For the effect of adsorbent dosage, an increase in Pb(II) removal can be linked over the increase of active sites accessibility upon the increasing of adsorbent dosage (Gyananath et al., 2012). However, higher values of adsorbent dosage resulted in the formation of the adsorbent aggregation, thus decrease the viability of surface area for removal of Pb(II) (Kireeti et al., 2016).

The influence of initial concentration (X_1) and time (X_3) towards the Pb(II) removal percentage are shown in 3D plot of Figure 4.5(B). The Pb(II) withdrawal escalated (58-75%) with initial Pb(II) concentration (from 50 to 375 mg/L) and time (from 60 to 140 min) until the optimum initial concentration of 250 mg/L – 375 mg/L and time of 100 – 140 min were achieved with Pb(II) removal of 74-75%, but slightly decreased (70-64%) at higher values. For the effect of adsorption time, the escalating Pb(II) removal percentage at the beginning might be related to a high active site accessibility on the surface of KCC-1, meanwhile, a slower adsorption rate at the final stage might be due to the decreasing of active site on the surface of KCC-1 (Ekka et al., 2015). Thus, the percentage Pb(II) removal decreased after the optimum time achieved. Kalantari et al. (Kalantari et al., 2014) also described the similar trend in the study of the effect of initial concentration and time on Pb(II) elimination onto Fe_3O_4/Talc nanocomposite.

Figure 4.5(C) shows the influence of adsorbent dosage (X_2) and time (X_3) towards Pb(II) removal percentage in 3D plot. The graph indicates that, the increment in time (from 60 to 140 min) and adsorbent dosage (0.5 to 3 g/L) led to the increase (58-75%) in Pb(II) removal percentage but decreased (66-60%) after the optimum conditions (X_2 = 1.5 – 3 g/L, X_2 = 100 – 140 min) were achieved. As illustrated in 3D plot, it is clearly observed that the interaction of X_2X_3 (Fig. 4(C)) insignificant influence the percentage Pb(II) removal onto KCC-1(RHA) as compared to the X_1X_2 (Fig. 4(A)) and X_1X_3 (Fig. 4(B)) in agreement with the higher value of *p*-value of X_2X_3 as compared to the X_1X_2 and X_1X_3 as shown in Fig. 4. The result observed indicated that the interaction of X_1X_2 plays

a minor role in the Pb(II) adsorption process onto KCC-1. The influence of adsorbent dosage and time towards Pb(II) elimination was in agreement with Asfaram et al. (2015) in study of Mn-doped Fe_3O_4-NPs loaded on AC for removal of methylene blue (MB), Pb^{2+}, Cr^{3+} and Safranin-O (SO).

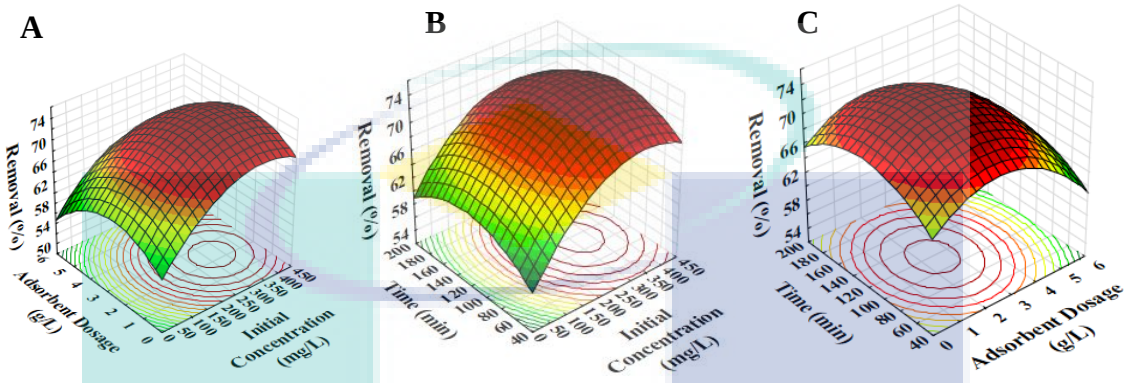

Figure 4.5 3D surface plots of percentage Pb(II) removal onto KCC-1(RHA) predicted from the quadratic model: (A) initial concentration – adsorbent dosage interaction, (B) initial concentration – time interaction, and (C) adsorbent dosage – time interaction.

From this statistical analysis study, the optimum condition of variables; Pb(II) initial concentration, adsorbent dosage of KCC-1 and time of process were found to be at 322.06 mg/L, 2.4 g/L, and 117 min, respectively, with the predicted percentage Pb(II) removal of 74.50%. The Pb(II) removal onto KCC-1 were carried out using the optimum conditions to validate the significance of the result. From the experiment, 75% of Pb(II) was successfully removed from the aqueous solution over KCC-1 with 0.5% error. Additional experiments were carried out by employing the KCC-1(C) and KCC-1 prepared from TEOS (KCC-1(TEOS)) as comparison. The percentage of Pb(II) removal using KCC-1(C) and KCC-1(TEOS) was 77% and 81%, which slightly higher than that of KCC-1(RHA). A small difference in the percentage of Pb(II) removal might be related with the higher purity of the commercial silica source originated from Na_2SiO_3-C and TEOS as compared to the Na_2SiO_3-RHA.

4.3 Adsorption Kinetics

Adsorption kinetics is a study that explains the mechanism which control the adsorption activity like chemical reaction and mass transfer. In this study, three types of kinetic models (pseudo-first order (Lagergren, 1898), pseudo-second order (Ho & McKay, 1999), and Elovich kinetic (Wu & Juang, 2014)) were used to fit the

experimental data of Pb(II) adsorption onto KCC-1. In detail, pseudo-first order and pseudo second-order described the behavior of adsorption which in physisorption or chemisorption, respectively, while, Elovich model explained the kinetics of heterogeneous chemisorption (Salim & Munekage, 2009). The equation of the models was expressed as follow:

Pseudo-first order model:
$$\log(q_e - q_t) = \log q_e - \frac{k_1}{2.303} t \quad (4.2)$$

Pseudo-second order model:
$$\frac{t}{q_t} = \frac{1}{k_2 q_e^2} + \frac{1}{q_e} t \quad (4.3)$$

Elovich kinetic:
$$q_e = \left(\frac{1}{\beta}\right) \ln(\alpha\beta) + \left(\frac{1}{\beta}\right) \ln t \quad (4.3)$$

where q_t and q_e is the values of Pb(II) adsorbed at time, t, and equilibrium (mg/g), respectively, k_2 is the rate constant of pseudo-second order adsorption (g/mg.min), k_1 is the rate constant of pseudo-second order adsorption (L/min), β is desorption constant during the experiment (g/mg) and α is the adsorption rate constant (mg/(g.min)).

The calculated data from each model was tabulated and summarized in Table 4.3. From the data, the suitable kinetic study increased with the trend of pseudo-second order > pseudo first order > Elovich. The pseudo-second-order was chosen as the kinetic model best-fitted to the experimental data owing to the highest regression coefficient, R^2 (≥ 0.9985) and closed value of q_e to the experimental value compared with the others. Meanwhile, Elovich model represented the weakest model for investigating the Pb(II) adsorption capacity over KCC-1 due to the lowest R^2 value as compared to the others. As the adsorption process followed the pseudo-second-order model, it is reasonable to claim that the chemisorption process and the rate of reaction were dominant over the adsorption process of Pb(II) onto KCC-1 and even directly proportional to the active sites accessiblity on the adsorbent surface. Comparable findings were also declared for the Pb(II) adsorption onto another mesoporous silica such amino-functionalized fly-ash-based SBA-15 mesoporous molecular (Li et al., 2017), 1-alkyl-3-methylimidazolium bromide ionic liquid mediated mesoporous silica (Ekka et al., 2015), and bis-pyrazolyl functionalized mesoporous silica and MCM-41 functionalized with amine (Cui et al., 2017). They found that the experimental data was comparable with the pseudo-second-

order model due to the high value of regression coefficient R^2, suggested the chemisorption process controlled the adsorption process.

Table 4.3 Kinetic parameters for Pb(II) removal onto KCC-1(RHA).

Models	Parameter	100 ppm	200 ppm	300 ppm	400 ppm	500 ppm
Experimental	$q_{e,exp}$ (mg/g)	13.374	19.069	23.122	42.617	48.978
Pseudo-first-order	$q_{e,cal}$ (mg/g)	11.612	10.462	9.874	10.440	15.237
	k_1 (min^{-1})	0.0355	0.0272	0.0389	0.0269	0.0193
	R^2	0.9937	0.9925	0.9097	0.9964	0.9927
Pseudo-second-order	$q_{e,cal}$ (mg/g)	15.456	20.284	24.331	43.103	50.761
	k_2 (g/mg·min)	0.0032	0.0050	0.0080	0.0066	0.0035
	R^2	0.9990	0.9954	0.9985	0.9978	0.9950
Elovich kinetic	α (mg/(g.min))	3.32	58.00	740.64	5E+06	5E+04
	β (g/mg)	0.3923	7.3328	0.4582	0.4761	0.3090
	R^2	0.9530	0.9189	0.8764	0.9056	0.8349

4.4 Adsorption Isotherm

The adsorption system and the mechanism of the solutes interacted with the adsorbent was depicted by the adsorption isotherm. In this study, the isotherm model of Freundlich (Freundlich, 1906), Langmuir (Langmuir, 1918), Temkin (Dubinin, 1906) and Dubinin-Radushkevich (Tempkin & Pyzhev, 1940) and were used for analyzing the experimental data. In brief, Langmuir isotherm is linked to the connection between the adsorbate concentration in the solution and the presence of active sites on the surface of adsorbent at equilibrium. Once the adsorbate being adsorbed onto the adsorbent surface occurred, it might create a monolayer formation on the homogenous adsorbent surface which then affected towards no further adsorption (Javadian et al., 2017). Besides, Freundlich isotherm was commonly used for the multilayer adsorption over the heterogeneous surface of adsorbent (Asfaram et al., 2015). Meanwhile, Temkin was used to study the effect of interactions amongst adsorbate and adsorbent in adsorption (Günay, Arslankaya, & Tosun, 2007) and it was reported that these adsorbate-adsorbent interactions might produce a decreasing of molecules heat adsorption within the layer linearly due to coverage of adsorbent surfaces. On the other hand, Dubinin-Radushkevich isotherm was related to the adsorption mechanism based on the heterogeneous surface assumption theory (Vijayalakshmi et al., 2017). The linearized forms of these isotherms were expressed as below:

Langmuir: $$\frac{C_e}{q_e} = \frac{1}{q_m K_L} + \frac{C_e}{q_m} \quad (4.4)$$

Freundlich: $$\log q_e = \log K_F + \frac{1}{n} \log C_e \quad (4.5)$$

Temkin: $$q_e = B \ln A + B \ln C_e \quad (4.6)$$

Dubinin-Radushkevich: $$\ln q_e = \ln q_m - K_{DR} \varepsilon^2 \quad (4.7)$$

where q_e and q_m (mg/g) is the adsorption capacity at equilibrium and the maximum adsorption capacity, respectively, n is an empirical constant, C_e (mg/L) is the Pb(II) concentration at equilibrium, K_L (L/mg) and K_F ((mg/g)(L/mg)$^{1/n}$)) is the Langmuir and Freundlich constant, respectively. B is the Temkin constant, A (L/g) is the Temkin equilibrium binding constant, K_{DR} (mol^2/kJ^2) is Dubinin-Radushkevich constant and ε (J/mol) is the Polanyi potential in which can be determined from $\varepsilon = RT \ln (1+1/C_e)$, where R is gas constant (8.314 J/mol·K) and T (K) is absolute temperature. The dimensionless constant separation factor, R_L, which is given by $R_L = 1/(1+K_L C_o)$ (Günay et al., 2007) were an important properties of the Langmuir isotherm. The R_L parameter which indicates the isotherm shape probably either unfavourable ($R_L > 1$), linear ($R_L = 1$), favourable ($0 < R_L < 1$) or irreversible ($R_L = 0$) (Günay et al., 2007) was considered as more reliable indicator for the adsorption process.

The calculated values using the formula of Langmuir, Freundlich, Temkin, and Dubinin-Radushkevich parameter was presented in Table 4. Analysis of the R^2 values suggested the Pb(II) adsorption onto KCC-1 followed the Langmuir isotherm model due to highest R^2 value ($\geq$0.9917), indicating monolayer adsorption occurred on the homogenous surface of adsorbent. From the Table 4, the Langmuir q_m value, K_L constant, R_L value was 46.729 mg/g, 0.0710 L/mg, and 0.1235, respectively. The observed results confirmed that the prepared KCC-1 was significantly favorable for the Pb(II) adsorption under conditions (Pb(II) initial concentration = 322.06 mg/L, adsorbent dosage of KCC-1 = 2.4 g/L and time = 117 min) used in this study. Langmuir isotherm was also reported as the best isotherm model for the elimination of Pb(II) onto Chitosan Beads (Gyananath et al., 2012), bis-pyrazolyl functionalized mesoporous silica and MCM-41 functionalized with amine (Cui et al., 2017), and amino-functionalized fly-ash-based SBA-15 mesoporous molecular (Li et al., 2017) with $R^2 \geq 0.9$.

Table 4.4 Isotherm models for Pb(II) adsorption onto KCC-1(RHA).

Isotherm model	**Parameters**	**Value**
Langmuir	q_m (mg/g)	26.954
	K_L (L/mg)	0.0112
	R^2	0.9934
	R_L	0.4705
Freundlich	n	0.5109
	K_f (mg/g)(L/mg)$^{1/n}$	58.790
	R^2	0.9860
Temkin	B (J/mol)	53.826
	A (L/g)	24.604
	R^2	0.9287
Dubinin-Radushkevich	q_m (mg/g)	69.318
	K_{ad} (10^{-4})	1
	R^2	0.9634

Additional adsorption isotherm studies were executed by employing the KCC-1(C) and KCC-1(TEOS) as comparison. The q_m values for KCC-1(RHA), KCC-1(C) and KCC-1(TEOS) was compared with other silica types adsorbents reported in literatures for Pb(II) removal as listed in Table 5. It is clearly observed that KCC-1 has higher adsorption capacity compared with other adsorbents, which might be due to the unique features of the KCC-1, indicating a great potential of KCC-1 to be used as adsorbent for removal of Pb(II).

Table 4.5 Comparison of Pb(II) adsorption capacity of several types of silica absorbent.

Adsorbent	**Adsorption capacity (mg/g)**	**Ref**
KCC-1(RHA)	26.954	This study
KCC-1(C)	30.889	This study
KCC-1(TEOS)	38.760	This study
Amine-functionalised SBA-15	0.030	(McManamon et al., 2012)
HMS-SH	0.100	(MacHida et al., 2012)
HMS-NH_2	0.430	(MacHida et al., 2012)
Silica Ceramic	2.7586	(Salim & Munekage, 2009)
1-alkyl-3-methylimidazolium bromide	5.1813	(Ekka et al., 2015)
Activated Silica Gel (ASG)	15.620	(Kushwaha et al., 2017)
Thiophenecarbonyl Loaded Silica Gel (TLSG)	17.850	(Kushwaha et al., 2017)
2-Furoyl Loaded Silica Gel (FLSG)	19.600	(Kushwaha et al., 2017)
L-Proline Loaded Silica Gel (PLSG)	22.220	(Kushwaha et al., 2017)

4.5 Regeneration and Reusability

The Pb(II) adsorption during five adsorption-desorption cycles are shown in Fig. 6. The desorption process was studied using a chemical treatment of 0.1 M nitric acid due to a good performance of nitric acid as compared to the hydrochloric acid and sodium hydroxide as reported by Kour (Kour, 2016). In brief, desorption process was carried out by contacting a metal ions - saturated dry adsorbent under agitation at room temperature (30°C). From the experiment, the adsorption-desorption of Pb(II) was declined with increasing number of the cycle, suggesting some of the active sites were blocked by the Pb(II) and the changes in the structure and the chemistry of adsorbent (Vijayalakshmi et al., 2017). A decreasing in the percentage of Pb(II) adsorption during multiple cycle was in agreement with Kireeti et al. (Kireeti et al., 2016) on a adsorption-desorption of sodium modified reduced graphene oxide-magnetic iron oxide (rGO-Fe_3O_4) nanocomposite for Pb(II) removal using five cycles.

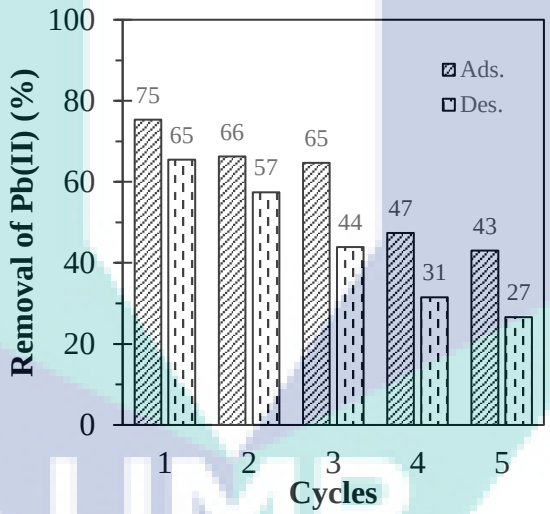

Figure 4.6 Adsorption-desorption for removal of Pb(II) onto KCC-1(RHA).

The FTIR spectra of KCC-1 before and after five cycles of adsorption-desorption of Pb(II) are shown in Fig. 7. The existence of peak at 3399 cm^{-1}, 1063 cm^{-1}, 799 cm^{-1}, and 448 cm^{-1} represented O-H stretching vibration of Si-OH, symmetrical stretching of Si-O, unsymmetrical stretching of Si-O, and Si-O bending, respectively (Ekka et al., 2015). After the adsorption process, the peaks slightly shifted to lower frequencies which were from 3399 cm^{-1} to 3395 cm^{-1}, 1063 cm^{-1} to 1055 cm^{-1}, 799 cm^{-1} to 797 cm^{-1} and 448 cm^{-1} to 446 cm^{-1}, respectively, indicating the interaction of functional groups in the metal

binding process. The alteration of peak at 3399 cm^{-1} to 3395 cm^{-1} might be related to the formation of Si-O-Pb upon the Pb(II) adsorption from the aqueous solution (Kuncoro & Fahmi, 2013). Dolphen & Thiravetyan (2011) have reported that the shifted of the FTIR bands upon adsorption were due to the electrostatic and chemical adsorption. Besides, Beh et al. (2012) also reported that the shifted of peaks might related to the complexation and coordination of functional group with metal ions.

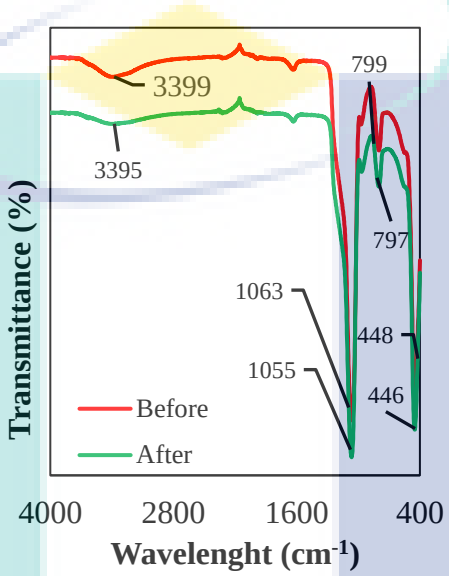

Figure 4.7 FTIR spectra of KCC-1(RHA) before and after five cycles of adsorption-desorption towards Pb(II) removal.

CHAPTER 5

CONCLUSION

5.1 Conclusion

In the present study, KCC-1(RHA) were successfully synthesized using alternative silica precursor which was the sodium silicate extracted from rice husk ash (RHA) (Na_2SiO_3-RHA). Preliminary study was carried out to study the effect of acid leaching towards the amount of silica (SiO_2) content. The result showed that the leached-RHA contained higher percentage of SiO_2 (95.44%) as compared to un-leached RHA (88.52%), owing to the removal of inorganic impurities during leaching process. Preparation of Na_2SiO_3-RHA via alkaline fusion method was successful removed 6% of silica.

The synthesized KCC-1(RHA)) were characterized using TEM, XRD, FTIR, and BET. The characterization results revealed that the synthesized KCC-1(RHA)) have fibrous silica structure with high surface area (220 m^2/g) which comparable with KCC-1 synthesized from commercial silica source, KCC-1(C) (227 m^2/g). The FTIR result showed the present of O-H stretching vibration of Si-OH, symmetrical stretching of Si-O, unsymmetrical stretching of Si-O, and Si-O bending, indicating the successful synthesized of KCC-1(RHA).

The effect of initial concentration, X_1 (50 – 400 mg/L), adsorbent dosage, X_2 (0.5 – 5.0 g/L) and time, X_3 (60 – 180 min) towards Pb(II) removal, Y, were optimized using response surface methodology (RSM). The optimum conditions were found to be X_1 = 322.06 mg/L, X_2 = 2.4 g/L and X_3 = 117 min, with Y = 74.50%. The pareto chart revealed that the linear term of initial concentration (X_1) was the most noteworthy parameter for removal of Pb(II) using KCC-1(RHA), while the linear term of time (X_3) was the least noteworthy factor for the Pb(II) removal.

The isotherm, kinetic, and reusability study was carried out at optimum condition. The experimental data fitted well with Langmuir isotherm model indicating monolayer adsorption occurred on the homogenous surface of the adsorbent. Pseudo-second order kinetic model was best fitted the adsorption process, indicating the chemisorption process and the rate of reaction was directly proportional to the active sites accessibility on the KCC-1(RHA) surface. The adsorption-desorption test revealed that KCC-1(RHA) performs good adsorption-desorption for five cycles with reduction in percentage of Pb(II) removal from 75% to 43%, and 65% to 27% for adsorption and desorption, respectively, indicating a good potential of KCC-1(RHA) for the removal of Pb(II) from aqueous solution.

5.2 Recommendation for Future Work

The study of synthesis and characterization of functionalized KCC-1 prepared from rice husk ash (RHA) and its application in adsorption process still in the beginning. There are many things can be considered for future study of KCC-1 such as:

i. In adsorbent synthesis: Different types of co-surfactant such as pentanol and isopropanol can be examined for synthesizing KCC-1. The different types of co-surfactant will influence the physicochemical properties of KCC-1, and thus its activity towards adsorption process.
ii. In adsorbent synthesis: Other types of silica-rich waste materials such as Palm Oil Fuel Ash (POFA) and Fly ash can be used as silica precursor.

REFERENCES

Abadin, H., Ashizawa, A., Stevens, Y.-W., Llados, F., Diamond, G., Sage, G., Citra M., Quinones A., Bosch S. J., and Swarts, S. G. (2007). Toxicological Profile for Lead. U.S Public Health Service, Agency for Toxic Substances and Disease Registry, (August), 582.

Abbaszadeh, S., Alwi, S. R. W., Webb, C., Ghasemi, N., & Muhamad, I. I. (2016). Treatment of lead-contaminated water using activated carbon adsorbent from locally available papaya peel biowaste. Journal of Cleaner Production, 15–45.

Abubakar, A. U., & Baharudin, K. S. (2012). Potential Use of Malaysian Thermal Power Plants Coal Bottom Ash in Construction. International Journal of Sustainable Construction Engineering & Technology, 3(2), 2180–3242.

Ahmad, A. L., Harris, W. A., Syafiee, & Seng, O. B. (2007). Removal of Dye From Wastewater of Textile Industry Using Membrane Technology. Jurnal Teknologi, 36(F), 31–44.

Ahmad, R., & Hasan, I. (2016). Optimization of the adsorption of Pb (II) from aqueous solution onto PAB nanocomposite using response surface methodology. Environmental Nanotechnology, Monitoring and Management, 6, 116–129.

Ahmad, T., Rafatullah, M., Ghazali, A., Sulaiman, O., & Hashim, R. (2011). Oil palm biomass-based adsorbents for the removal of water pollutantsa review. Journal of Environmental Science and Health - Part C Environmental Carcinogenesis and Ecotoxicology Reviews, 29(3), 177–222.

Akinbayo Akinbiyi. (2000). Removal of Lead from Aqueous Solutions by Adsorption using Peat Moss, 1–101.

Al-Enezi, G., Hamoda, M. F., & Fawzi, N. (2004). Ion Exchange Extraction of Heavy Metals from Wastewater Sludges. Journal of Environmental Science and Health - Part A Toxic/Hazardous Substances and Environmental Engineering, 39(2), 455–464.

Al-Rashdi, B., Somerfield, C., & Hilal, N. (2011). Heavy Metals Removal Using Adsorption and Nanofiltration Techniques Heavy Metals Removal Using Adsorption and Nanofiltration Techniques. Separation and Purification Revuiew, 40, 209–259.

Alfredsson, V. (2015). Mesoporous materials- an overview. Mesoporous Material, 1, 1–58.

Almalih, M. A., Salih, A., Dafaallah, A. A., Magid, S. A. A., Gizouli, A. M. E., & Tilal, A. S. (2015). Removal of Heavy Metal Ions from Industrial Wastewater by Scolecite. Journal of Environmental & Analytical Toxicology, 5(5).

Alvarez, M. T., Crespo, C., & Mattiasson, B. (2007). Precipitation of Zn(II), Cu(II) and Pb(II) at bench-scale using biogenic hydrogen sulfide from the utilization of volatile

fatty acids. Chemosphere, 66(9), 1677–1683.

Anbia, M., & Hariri, S. A. (2010). Removal of methylene blue from aqueous solution using nanoporous SBA-3. Desalination, 261(1–2), 61–66.

Ardekani, P. S., Karimi, H., Ghaedi, M., Asfaram, A., & Purkait, M. K. (2017). Ultrasonic assisted removal of methylene blue on ultrasonically synthesized zinc hydroxide nanoparticles on activated carbon prepared from wood of cherry tree: Experimental design methodology and artificial neural network. Journal of Molecular Liquids, 229, 114–124.

Argiz C, Menéndez E, Moragues A, & Sanjuánc M. A. (2015). Fly ash characteristics of Spanish coal-fired power plants. Afinidad, 72, 269–277.

Asfaram, A., Ghaedi, M., Goudarzi, A., & Rajabi, M. (2015). Response surface methodology approach for optimization of simultaneous dye and metal ion ultrasound-assisted adsorption onto Mn doped Fe 3 O 4 -NPs loaded on AC: kinetic and isothermal studies. Dalton Trans., 44(33), 14707–14723.

Azad, F. N., Ghaedi, M., Asfaram, A., Jamshidi, A., Hassani, G., Goudarzi, A., … Ghaedi, A. (2016). Optimization of the process parameters for the adsorption of ternary dyes by Ni doped FeO(OH)-NWs–AC using response surface methodology and an artificial neural network. RSC Adv., 6(24), 19768–19779.

Basset, J.-M., Bailey, A. R., Amy Farago, T., McElwee, E., Polshettiwar, V., & Srinivasan, M. (2010). Fibrous Silica Nanospheres. Catal. Sci. Technology, 1, 1–2.

Bayal, N., Singh, B., Singh, R., & Polshettiwar, V. (2016). Size and Fiber Density Controlled Synthesis of Fibrous Nanosilica Spheres (KCC-1). Scientific Reports, 6(April), 24888.

Beddri, A. M. bin, & Ismail, Z. binti. (2007). Removal of Heavy Metals from Refinery Effluents using Water. JURUTERA, (March), 1–4.

Begum, R. A., Sohaga, K., Abdullah, S. M. S., & Jaafar, M. (2015). CO2 emissions, energy consumption, economic and population growth in Malaysia. Renewable and Sustainable Energy Reviews, 41, 594–601.

Beh, C. L., Chuah, T. G., M. N. Nourouzi, & Choong, T. S. Y. (2012). Removal of Heavy Metals from Steel Making Waste Water by Using Electric Arc Furnace Slag. Journal of Chemistry, 9(4), 2557–2564.

Berger, A. H., & Bhown, A. S. (2011). Comparing physisorption and chemisorption solid sorbents for use separating CO2 from flue gas using temperature swing adsorption. Energy Procedia, 4, 562–567.

Bezerra, M. A., Santelli, R. E., Oliveira, E. P., Villar, L. S., & Escaleira, L. A. (2008). Response surface methodology (RSM) as a tool for optimization in analytical chemistry. Talanta, 76(5), 965–977. https://doi.org/10.1016/j.talanta.2008.05.019

Bhagiyalakshmi, M., Yun, L. J., Anuradha, R., & Jang, H. T. (2010). Synthesis of chloropropylamine grafted mesoporous MCM-41, MCM-48 and SBA-15 from rice

husk ash: Their application to CO2 chemisorption. Journal of Porous Materials, 17(4), 475–484.

Buekens, A., & Zyaykina, N. N. (2001). Adsorbent and Adsorption Processes for Pollution Control. Pollution Control Technology, II, 1–10.

Byoun, W., Jung, S., Tran, N. M., & Yoo, H. (2018). Synthesis and Application of DEndritis Fibrous Nanosilica/Gold Nanomaterials. Chemistry Open, 7(5), 349–355.

Chen, Q., Luo, Z., Hills, C., Xue, G., & Tyrer, M. (2009). Precipitation of heavy metals from wastewater using simulated flue gas: Sequent additions of fly ash, lime and carbon dioxide. Water Research, 43(10), 2605–2614.

Cui, H. Z., Li, Y. L., Liu, S., Zhang, J. F., Zhou, Q., Zhong, R., … Hou, X. F. (2017). Novel Pb(II) ion-imprinted materials based on bis-pyrazolyl functionalized mesoporous silica for the selective removal of Pb(II) in water samples. Microporous and Mesoporous Materials, 241, 165–177.

Daffalla, S. B., Mukhtar, H., & Shaharun, M. S. (2012). Properties of activated carbon prepared from rice husk with chemical activation. International Journal of Global Environmental Issues, 12(2/3/4), 107.

Dhokte, A. O., Khillare, S. L., Lande, M. K., & Arbad, B. R. (2011). Synthesis, characterization of mesoporous silica materials from waste coal fly ash for the classical Mannich reaction. Journal of Industrial and Engineering Chemistry, 17(4), 742–746.

Diao, X., Wang, Y., Zhao, J., & Zhu, S. (2010). Effect of pore-size of mesoporous SBA-15 on adsorption of bovine serum albumin and lysozyme protein. Chinese Journal of Chemical Engineering, 18(3), 493–499.

Dolphen, R., & Thiravetyan, P. (2011). Adsorption of melanoidins by chitin nanofibers. Chemical Engineering Journal, 166(3), 890–895.

Dong, Z., Le, X., Dong, C., Zhang, W., Li, X., & Ma, J. (2015). Ni@Pd core-shell nanoparticles modified fibrous silica nanospheres as highly efficient and recoverable catalyst for reduction of 4-nitrophenol and hydrodechlorination of 4-chlorophenol. Applied Catalysis B: Environmental, 162, 372–380.

Dong, Z., Le, X., Li, X., Zhang, W., Dong, C., & Ma, J. (2014). Silver nanoparticles immobilized on fibrous nano-silica as highly efficient and recyclable heterogeneous catalyst for reduction of 4-nitrophenol and 2-nitroaniline. Applied Catalysis B: Environmental, 158–159, 129–135.

Dubinin, M. M. (1906). The potential theory of adsorption of gases and vapors for adsorbents with energetically non-uniform surface. Chemical Review, 60, 235–266.

Ekka, B., Rout, L., Sahu Aniket Kumar, M. K., Patel, R. K., & Dash, P. (2015). Removal efficiency of Pb(II) from aqueous solution by 1-alkyl-3-methylimidazolium bromide ionic liquid mediated mesoporous silica. Journal of Environmental Chemical Engineering, 3(2), 1356–1364.

F. C. Wu, R. L. T., & Juang, R. S. (2014). Characteristics of Elovich Equation Used for the Analysis of Adsorption Kinetics in Dye – Chitosan Systems. Chemical Enginnering Journal, 150, 366–373.

Fan, C. H., Chang, E. L., Ting, C. Y., Lin, Y. C., Liao, E. C., Huang, C. Y., … Yeh, C. K. (2016). Folate-conjugated gene-carrying microbubbles with focused ultrasound for concurrent blood-brain barrier opening and local gene delivery. Biomaterials, 106, 46–57.

Ferniza-garcía, F., Amaya-chávez, A., Roa-morales, G., & Barrera-díaz, C. E. (2017). Removal of Pb , Cu , Cd , and Zn Present in Aqueous Solution Using Coupled Electrocoagulation-Phytoremediation Treatment. International Journal of Electrochemistry, 2017(1), 1–12.

Ferreira, S. L. C., Bruns, R. E., da Silva, E. G. P., dos Santos, W. N. L., Quintella, C. M., David, J. M., Andrade J. B. D., Breitkreitz M. C., Jardim I. C. S. F., & Neto, B. B. (2007). Statistical designs and response surface techniques for the optimization of chromatographic systems. Journal of Chromatography A, 1158(1–2), 2–14.

Fihri, A., Bouhrara, M., Patil, U., Cha, D., Saih, Y., & Polshettiwar, V. (2012). Fibrous nano-silica supported ruthenium (KCC-1/Ru): A sustainable catalyst for the hydrogenolysis of alkanes with good catalytic activity and lifetime. ACS Catalysis, 2(7), 1425–1431.

Flora, G., Gupta, D., & Tiwari, A. (2012). Toxicity of lead: A review with recent updates. Interdisciplinary Toxicology, 5(2), 47–58.

Freundlich, H. (1906). Adsorption in solution. Journal of Physical Chemistry, 57, 47–385.

Fu, F., & Wang, Q. (2011). Removal of heavy metal ions from wastewaters: A review. Journal of Environmental Management, 92(3), 407–418.

Galameau, A., Cambon, H., Martin, T., De Ménorval, L.-C., Brunel, D., Di Renzo, F., & Fajula, F. (2002). SBA-15 versus MCM-41: are they the same materiais?, 2991(July 2015), 395–402.

George, G. (2018). Eco-friendly utilization of fly ash characterization. International Journal of Advances in Science Engineering and Technology, (1), 1–6.

Ghazy, S. E., El-Morsy M. S., & Ragab, A. H. (2008). Ion Flotation of Copper (II) and Lead (II) from Environmental Water Samples. Journal of Applied Sciences and Environmental Management, 12(3), 75–82.

Goyal, A., Kunio, H., & Hidehiko, O. (2016). Properties and reactivity of sugarcane bagasse ash. Research Journal of Biomass, 3(2), 1–2.

Günay, A., Arslankaya, E., & Tosun, I. (2007). Lead removal from aqueous solution by natural and pretreated clinoptilolite: Adsorption equilibrium and kinetics. Journal of Hazardous Materials, 146(1–2), 362–371.

Guo, Y., Liu, D., Zhao, Y., Gong, B., Guo, Y., & Huang, W. (2017). Synthesis of

chitosan-functionalized MCM-41-A and its performance in Pb(II) removal from synthetic water. Journal of the Taiwan Institute of Chemical Engineers, 71, 537–545.

Gustafsson, H., Isaksson, S., Altskär, A., & Holmberg, K. (2016). Mesoporous silica nanoparticles with controllable morphology prepared from oil-in-water emulsions. Journal of Colloid and Interface Science, 467, 253–260.

Gyananath, G., Balhal, D. K., & Sciences, L. (2012). Removal of Lead (II) from Aqueous Solution by Adsorption onto Chitosan Beads. Cellulose Chemistry and Technology, 46(Ii), 121–124.

Hajdu, I., Bodnár, M., Csikós, Z., Wei, S., Daróczi, L., & Kovács, B. (2012). Combined nano-membrane technology for removal of lead ions, 410, 44–53.

Hamid, M. Y. S., Firmansyah, M. L., Triwahyono, S., Jalil, A. A., Mukti, R. R., Febriyanti, E., Suendo V., Setiabudi H. D., Mohamed M., & Nabgan, W. (2017). Oxygen vacancy-rich mesoporous silica KCC-1 for CO2 methanation. Applied Catalysis A: General, 532, 86–94

Heidari, A., Younesi, H., & Mehraban, Z. (2009). Removal of Ni(II), Cd(II), and Pb(II) from a ternary aqueous solution by amino functionalized mesoporous and nano mesoporous silica. Chemical Engineering Journal, 153(1–3), 70–79.

Hernández-Morales, V., Nava, R., Acosta-Silva, Y. J., MacÍas-Sánchez, S. A., Pérez-Bueno, J. J., & Pawelec, B. (2012). Adsorption of lead (II) on SBA-15 mesoporous molecular sieve functionalized with -NH2groups. Microporous and Mesoporous Materials, 160, 133–142.

Ho, Y. S., & McKay, G. (1999). Pseudo-second order model for sorption processes. Journal of Process Biochemistry, 34(5), 451–465.

Huang, X., Tao, Z., Praskavich, J. C., Goswami, A., Al-Sharab, J. F., Minko, T., … Asefa, T. (2014). Dendritic silica nanomaterials (KCC-1) with fibrous pore structure possess high DNA adsorption capacity and effectively deliver genes in vitro. Langmuir, 30(36), 10886–10898.

Huirache-Acuña, R., Nava, R., Peza-Ledesma, C., Lara-Romero, J., Alonso-Núez, G., Pawelec, B., & Rivera-Muñoz, E. (2013). SBA-15 Mesoporous Silica as Catalytic Support for Hydrodesulfurization Catalysts—Review. Materials, 6(9), 4139–4167.

Isabella, A. N. A., & Pérez, N. (2015). Analysis and improvement proposal of a wastewater treatment plant in a Mexican refinery. Wastewater, 1, 1–71.

Issaraporn, S., & Chareonpanich, M. (2000). Modification of Pore Size of SBA-15 Mesoporous Silica Produced from Rice Husk Ash. Catal. Today, 1, 1–6.

Jadhav, K., Dumbare, P., & Pande, V. (2015). Mesoporous Silica Nanoparticles (MSN): A Nanonetwork and Hierarchical Structure in Drug Delivery. Journal of Nanomedicine Research, 2(5).

Jafari, S., Derakhshankhah, H., Alaei, L., Fattahi, A., Varnamkhasti, B. S., & Saboury,

A. A. (2018). Mesoporous silica nanoparticles for therapeutic/diagnostic applications. Biomedicine & Pharmacotherapy, 109(October 2018), 1100–1111.

Javadian, H., Koutenaei, B. B., Shekarian, E., Sorkhrodi, F. Z., Khatti, R., & Toosi, M. (2017). Application of functionalized nano HMS type mesoporous silica with N-(2-aminoethyl)-3-aminopropyl methyldimethoxysilane as a suitable adsorbent for removal of Pb (II) from aqueous media and industrial wastewater. Journal of Saudi Chemical Society, 21, S219–S230.

Jhadhav, K., Dumbare, P., & Pande, W. (2015). Mesoporous Silica Nanoparticles (MSN): A Nanonetwork and Hierarchical Structure in Drug Delivery. Journal of Nanomedicine Research, 2(5), 1–15.

Kahkha, M. R. R., Piri, J., & Kaykhaii, M. (2014). Application of Response Surface Modeling and Central Composition Design for Removal of Lead from Aqueous Solution Using Prosopis Stephanian Fruits. International Research Journal of Applied and Basic Science, 8(6), 701–706.

Kalantari, K., Ahmad, M. B., Masoumi, H. R. F., Shameli, K., Basri, M., & Khandanlou, R. (2014). Rapid adsorption of heavy metals by Fe3O4/talc nanocomposite and optimization study using response surface methodology. International Journal of Molecular Sciences, 15(7), 12913–12927.

Kavak, D. (2013). Removal of lead from aqueous solutions by precipitation: Statistical analysis and modeling. Desalination and Water Treatment, 51(7–9), 1720–1726.

Kempen, P. J., Greasley, S., Parker, K. A., Campbell, J. L., Chang, H. Y., Jones, J. R., … Jokerst, J. V. (2015). Theranostic mesoporous silica nanoparticles biodegrade after pro-survival drug delivery and ultrasound/magnetic resonance imaging of stem cells. Theranostics, 5(6), 631–642.

Keramati, N., Fallah, N., & Nasernejad, B. (2016). Application of response surface methodology for optimization of operational variables in photodegradation of aqueous styrene under visible light. Desalination and Water Treatment, 57(41), 19239–19247.

Kharub, M. (2012). Use of various technologies, methods and adsorbents for the removal of dye. Journal of Environemntal Research and Development, 6(3), 879–883.

Khataeea, a R., Kasirib, M. B., & Alidokht, L. (2011). Application of response surface methodology in the optimization of photocatalytic removal of environmental pollutants using nanocatalysts. Environmental Technology, 33(15–16), 1669–84.

Kireeti, K. V. M. K., G., C., Kadam, M. M., & Jha, N. (2016). A sodium modified reduced graphene oxide–Fe 3 O 4 nanocomposite for efficient lead(II) adsorption. RSC Adv., 6(88), 84825–84836.

Kour, J. (2016). Regeneration and reuse of biomaterial for the removal of cadmium ions from waste water. Journal of Institute of Science and Technology, 21(1), 90–94.

Kuncoro, E. P., & Fahmi, M. Z. (2013). Removal of Hg and Pb in Aqueous Solution using Coal Fly Ash Adsorbent. Procedia Earth and Planetary Science, 6, 377–382.

Kushwaha, A. K., Gupta, N., & Chattopadhyaya, M. C. (2017). Adsorption behavior of lead onto a new class of functionalized silica gel. Arabian Journal of Chemistry, 10, S81–S89.

Langmuir, I. (1918). The adsorption of gases on plane surfaces of glass, mica and platinum. Journal of America Chemical Society, 40, 1361–1403.

Latchubugata, C. S., Kondapaneni, R. V., Patluri, K. K., Virendra, U., & Vedantam, S. (2018). Kinetics and optimization studies using Response Surface Methodology in biodiesel production using heterogeneous catalyst. Chemical Engineering Research and Design, 135, 129–139.

Le, X., Dong, Z., Zhang, W., Li, X., & Ma, J. (2014). Fibrous nano-silica containing immobilized Ni@Au core-shell nanoparticles: A highly active and reusable catalyst for the reduction of 4-nitrophenol and 2-nitroaniline. Journal of Molecular Catalysis A: Chemical, 395, 58–65.

Lemley, A., Wagenet, L., & Kneen, B. (1995). Activated Carbon Treatment of Drinking Water. Water Treatment Notes: Cornell Cooperative Extension, College of Human Ecology, 1–6.

Li, G., Wang, B., Sun, Q., Xu, W. Q., & Han, Y. (2017). Adsorption of lead ion on amino-functionalized fly-ash-based SBA-15 mesoporous molecular sieves prepared via two-step hydrothermal method. Microporous and Mesoporous Materials, 252, 105–115.

Lingamdinne, L. P., Koduru, J. R., Chang, Y.-Y., & Karri, R. R. (2018). Process optimization and adsorption modeling of Pb(II) on nickel ferrite-reduced graphene oxide nano-composite. Journal of Molecular Liquids, 250, 202–211.

MacHida, M., Fotoohi, B., Amamo, Y., & Mercier, L. (2012). Cadmium(II) and lead(II) adsorption onto hetero-atom functional mesoporous silica and activated carbon. Applied Surface Science, 258(19), 7389–7394.

Madamba, P. S. (2002). The response surface methodology: An application to optimize dehydration operations of selected agricultural crops. LWT - Food Science and Technology, 35(7), 584–592.

Mäkelä, M. (2017). Experimental design and response surface methodology in energy applications: A tutorial review. Energy Conversion and Management, 151(May), 630–640.

Malik, D. S., Jain, C. K., & Yadav, A. K. (2016). Removal of heavy metals from emerging cellulosic low-cost adsorbents: a review. Applied Water Science, 1–24.

Marcin, K., Jarosław, W., Monika, P., & Agnieszka, W. (2016). Application of the response surface methodology in optimizing oat fiber particle size and flour replacement in wheat bread rolls. CYTA - Journal of Food, 14(1), 18–26.

McManamon, C., Burke, A. M., Holmes, J. D., & Morris, M. A. (2012). Amine-functionalised SBA-15 of tailored pore size for heavy metal adsorption. Journal of Colloid and Interface Science, 369(1), 330–337.

Merganpour, A. M., Nekuonam, G., Tomaj, O. A., Kor, Y., & Safari, H. (2015). Efficiency of lead removal from drinking water using cationic resin Purolite. Environmental Health Engineering and Management Journal, 2(1), 41–45.

Mohammed, A. A., Ebrahim, S. E., & Alwared, A. I. (2013). Flotation and Sorptive-Flotation Methods for Removal of Lead Ions from Wastewater Using SDS as Surfactant and Barley Husk as Biosorbent, 2013.

Moi, F., Kumar, P., Tow, T., Omar, A. K. M., & Wasewar, K. L. (2011). Removal of lead , zinc and iron by coagulation – flocculation. Journal of the Taiwan Institute of Chemical Engineers, 42(5), 809–815. https://doi.org/10.1016/j.jtice.2011.01.009

Moyo, M., Chikazaza, L., Nyamunda, B. C., & Guyo, U. (2013). Adsorption Batch Studies on the Removal of Pb (II) Using Maize Tassel Based Activated Carbon. Journal of Chemistry, 2013, 1–8.

Naowanon, W., Chueachot, R., Klinsrisuk, S., & Amnuaypanich, S. (2018). Biphasic synthesis of amine-functionalized mesoporous silica nanospheres (MSN-NH2) and its application for removal of ferrous (Fe2 +) and copper (Cu2 +) ions. Powder Technology, 323, 548–557.

Nazni, P., & Gracia, J. (2014). Application of Response Surface Methodology in the Development of Barnyard Millet Bran Incorporated Bread. International Journal of Innovative Research in Science, Engineering and Technology, 03(09), 16041–16048.

Niu, B., Zhou, Y., Wen, T., Quan, G., Singh, V., Pan, X., & Wu, C. (2018). Proper functional modification and optimized adsorption conditions improved the DNA loading capacity of mesoporous silica nanoparticles. Colloids and Surfaces A: Physicochemical and Engineering Aspects, 548(March), 98–107.

Noor Syuhadah, S., & Rohasliney, H. (2012). Rice Husk as biosorbent: A Review. Health and the Environment Journal, 3(1), 89–95.

Norsuraya, S., Fazlena, H., & Norhasyimi, R. (2016). Sugarcane Bagasse as a Renewable Source of Silica to Synthesize Santa Barbara Amorphous-15 (SBA-15). Procedia Engineering, 148, 839–846.

Omatola, K. M., & Onojah, A. D. (2009). Elemental analysis of rice husk ash using X – ray fluorescence technique. International Journal of Physical Sciences, 4(4), 189–193.

Oshima, S., Perera, J. M., Northcott, K. A., Kokusen, H., Stevens, G. W., & Komatsu, Y. (2006). Adsorption behavior of cadmium(II) and lead(II) on mesoporous silicate MCM-41. Separation Science and Technology, 41(8), 1635–1643.

Pam, A. A., Abdullah, A. H., Ping, T. Y., & Zainal, Z. (2018). Batch and fixed bed adsorption of Pb(II) from aqueous solution using EDTA modified activated carbon derived from palm kernel shell. BioResources, 13(1), 1235–1250.

Pan, G., Jia, T. ting, Huang, Q. xia, Qiu, Y. yan, Xu, J., Yin, P. hao, & Liu, T. (2017). Mesoporous silica nanoparticles (MSNs)-based organic/inorganic hybrid

nanocarriers loading 5-Fluorouracil for the treatment of colon cancer with improved anticancer efficacy. Colloids and Surfaces B: Biointerfaces, 159, 375–385.

Parmar, M., & Thakur, L. S. (2013). Heavy metal Cu , Ni and Zn : Toxicity , health hazards and their removal techniques by low cost adsorbents : a short overview. International Journal of Plant, Animal and Environmental Sciences, 3(3), 143–157.

Patil, R., Dongre, R., & Meshram, J. (2014). Preparation of Silica Powder from Rice Husk. IOSR Journal of Applied Chemistry, 2014, 26–29.

Quan, G., Pan, X., Wang, Z., Wu, Q., Li, G., Dian, L., Chen, B., & Wu, C. (2015). Lactosaminated mesoporous silica nanoparticles for asialoglycoprotein receptor targeted anticancer drug delivery. *Journal of Nanobiotechnology*, *13*(1), 1–12.

Qureshi, Z. S., Sarawade, P. B., Hussain, I., Zhu, H., Al-Johani, H., Anjum, D. H., … Basset, J. M. (2016). Gold Nanoparticles Supported on Fibrous Silica Nanospheres (KCC-1) as Efficient Heterogeneous Catalysts for CO Oxidation. ChemCatChem, 8(9), 1671–1678.

Rahman, N. B. A., Rasid, H. M., Hassan, H. M., & Jalil, M. N. (2016). Synthesis and characterization of mesoporous silica mcm-41 and sba-15 from power plant bottom ash. Malaysian Journal of Analytical Sciences, 20(3), 539–545.

Rajput, M. S., Sharma, A. K., Sharma, S., & Verma, S. (2015). Removal of Lead (II) from aqueous solutions by orange peel. Internaltional Journal of Applied Research, 1(9), 411–413.

Rashed, M. N. (2013). Adsorption Technique for the Removal of Organic Pollutants from Water and Wastewater. Organic Pollutants - Monitoring, Risk and Treatment, 167–194.

Ravikumar, K., Kim, S. H., & Son, Y. A. (2007). Design of experiments for the optimization and statistical analysis of Berberine finishing of polyamide substrates. Dyes and Pigments, 75(2), 401–407.

Reddy, D. V., & Marcelina, B. S. A. (2006). Marine Durability Characteristics of Rice Husk Ash-Modified Reinforced. Laccet'2006, (June), 21–23.

S. Lagergren. (1898). About the theory of so-called adsorption of soluble substances. Journal of Chemical Engineering, 24(1), 1–39.

Sadhukhan, B., Mondal, N. K., & Chattoraj, S. (2016). Optimisation using central composite design (CCD) and the desirability function for sorption of methylene blue from aqueous solution onto Lemna major. Karbala International Journal of Modern Science, 2(3), 145–155.

Sakkas, V. A., Islam, M. A., Stalikas, C., & Albanis, T. A. (2010). Photocatalytic degradation using design of experiments: A review and example of the Congo red degradation. Journal of Hazardous Materials, 175(1–3), 33–44.

Salim, M. D., & Munekage, Y. (2009). Lead Removal from Aqueous Solution Using Silica Ceramic: Adsorption Kinetics and Equilibrium Studies. International Journal

of Chemistry, 1(1), 23–30.

Samal, K., Das, C., & Mohanty, K. (2016). Journal of Water Process Engineering Development of hybrid membrane process for Pb bearing wastewater treatment. Journal of Water Process Engineering, 10, 30–38.

Sarda, V., Handa, A. C., & Arora, K. K. (2015). Surface Chemistry. Chemistry (Vol. 16).

Saruchi, & Kumar, V. (2016). Adsorption kinetics and isotherms for the removal of rhodamine B dye and Pb+2 ions from aqueous solutions by a hybrid ion-exchanger. Arabian Journal of Chemistry.

Setiabudi, H. D., Jalil, A. A., Triwahyono, S., Kamarudin, N. H. N., & Jusoh, R. (2013). Ir / Pt-HZSM5 for n -pentane isomerization : Effect of Si / Al ratio and reaction optimization by response surface methodology. Chemical Engineering Journal, 217, 300–309.

Sett, R. (2017). Flyash : Characteristics , Problems and Possible Utilization Rupnarayan Sett *, 8(3), 32–50.

Sharahi, F. J., & Shahbazi, A. (2017). Melamine-based dendrimer amine-modified magnetic nanoparticles as an efficient Pb(II) adsorbent for wastewater treatment: Adsorption optimization by response surface methodology. Chemosphere, 189, 291–300.

Sharma, T., Toor, A. P., & Rajor, A. (2015). Photocatalytic degradation of imidacloprid in soil: application of response surface methodology for the optimization of parameters. RSC Adv., 5(32), 25059–25065.

Shon, H. K., Vigneswaran, S., Kandasamy, J., & Cho, J. (2008). Membrane technology for organic removal in wastewater. Water and wastewater treatment technologies, (1), 1–46.

Siddiqui, Z. N., Khan, K., & Ahmed, N. (2014). Nano fibrous silica sulphuric acid as an efficient catalyst for the synthesis of β-enaminone. Catalysis Letters, 144(4), 623–632.

Sijakova-ivanova, T., Panov, Z., Blazev, K., & Zajkova-paneva, V. (2011). Investigation of fly ash heavy metals content and physico chemical properties from thermal power plant , republic of macedonia. International Journal of Engineering Science and Technology, 3(12), 8219–8225.

Singh, B., & Polshettiwar, V. (2016). Design of CO 2 sorbents using functionalized fibrous nanosilica (KCC-1): insights into the effect of the silica morphology (KCC-1 vs. MCM-41). J. Mater. Chem. A, 4(18), 7071–7086.

Singh, K., Renu, N. A., & Agarwal, M. (2017). Methodologies for removal of heavy metal ions from wastewater: an overview. Interdisciplinary Environmental Review, 18(2), 124.

Sriatun, Taslimah, & Suyati, L. (2018). Synthesis of zeolite from sugarcane bagasse ash using cetyltrimethylammonium bromide as structure directing agent. Indonesian

Journal of Chemistry, 18(1), 159–165.

Sundaravadivel, D., & R Mohana. (2018). Recent Studies of Sugarcane Bagasse Ash in Concrete and Mortar- A Review. International Journal of Engineering Research & Technology, 7(04), 306–313.

Szponder, D. K., & Trybalski, K. (2011). Fly ash in agriculture - modern applications of coal combustion by-products, 373–385.

Tan, I. V. Y., & Wei, a I. (2008). Preparation , Characterization and Evaluation of Mesoporous Activated Carbons Derived From Agricultural By-Products for Adsorption of, 1, 1–55.

Tavallali, H., & Shiri, M. (2012). Solid phase extraction pf phenol from wastewater by magnetic iron oxide nanoparticles. International Journal of Chemical Research, 4(1), 311–318.

Teka, T., & Enyew, S. (2014). Study on effect of different parameters on adsorption efficiency of low cost activated orange peels for the removal of methylene blue dye. International Journal of Innovation and Scientific Research, 8(1), 106–111.

Tempkin, M. I., & Pyzhev, V. (1940). Kinetics of ammonia synthesis on promoted iron catalyst, Acta Physico- Chimica Sinica. USSR, 12, 327–356. Retrieved from

Thielemann, J., Girgsdies, F., Schlögl, R., & Hess, C. (2011). Pore structure and surface area of silica SBA-15: influence of washing and scale-up. Beilstein Journal of Nanotechnology, 2(1), 110–8.

Thilagavathy, P., & Santhi, T. (2012). Adsorption of Cr (VI) Onto Low-Cost Adsorbent Developed from Acacia Nilotica Leaf Activated with Phosphoric Acid: Kinetic, Equilibrium Isotherm and Thermodynamic Studies. International Journal of Science and Research (IJSR) ISSN (Online Impact Factor, 3(5), 2319–7064.

Todkar, B. S., Deorukhkar, O. A., & Deshmukh, S. M. (2016). Extraction of Silica from Rice Husk Ash. International Journal of Engineering Research and Development, 12(3), 69–74.

Tripathi, A., & Ranjan, M. R. (2015). Heavy Metal Removal from Wastewater Using Low Cost Adsorbents. Journal of Bioremediation & Biodegradation, 06(06), 1–5. 5

United Stated Environement Protection Agency. (1979). U.S. EPA. Environmental Pollution. EPA , Cincinnati, Ohio, 625/5, 79–106.

Vadia, N., & Sadhana, R. (2011). Mesoporous Material, Mcm- 41: a New Drug Carrier. Asian Journal of Pharmaceutical and Clinical Research, 4(2), 44–53.

Vijayalakshmi, K., Devi, B. M., Latha, S., Gomathi, T., Sudha, P. N., Venkatesan, J., & Anil, S. (2017). Batch adsorption and desorption studies on the removal of lead (II) from aqueous solution using nanochitosan/sodium alginate/microcrystalline cellulose beads. International Journal of Biological Macromolecules, 104, 1483–1494.

Wang, J., Fang, L., Cheng, F., Duan, X., & Chen, R. (2016). Hydrothermal Synthesis of SBA-15 Using Sodium Silicate Derived from Coal Gangue. Journal of Nanomaterials, 24, 1–6.

Wani, T. A., Ahmad, A., Zargar, S., Khalil, N. Y., & Darwish, I. A. (2012). Use of response surface methodology for development of new microwell-based spectrophotometric method for determination of atrovastatin calcium in tablets. Chemistry Central Journal, 6(1), 1–9.

Wenchao, Y. U., Yadan, G. U. O., Bai, G. A. O., & Ping, L. (2016). Research Advances of Chemical Treatment of Wastewater with Low Concentration of Uranium, (Icmmct), 235–239.

World Health Organization. (1984). Guidelines for Drinking Water Quality. World Health Organization, Geneva, Switzerlandland, 1–2.

Xu, C., Cao, L., Zhao, P., Zhou, Z., Cao, C., Li, F., & Huang, Q. (2018). Emulsion-based synchronous pesticide encapsulation and surface modification of mesoporous silica nanoparticles with carboxymethyl chitosan for controlled azoxystrobin release. Chemical Engineering Journal, 348(February), 244–254.

Yan, F., Jiang, J., Tian, S., Liu, Z., Shi, J., Li, K., Chen, X., & Xu, Y. (2016). A Green and Facile Synthesis of Ordered Mesoporous Nanosilica Using Coal Fly Ash. *ACS Sustainable Chemistry & Engineering*, *4*(9), 4654–4661.

Yi, Z., Yao, J., Zhu, M., Chen, H., Wang, F., & Liu, X. (2016). Kinetics , equilibrium , and thermodynamics investigation on the adsorption of lead (II) by coal - based activated carbon. SpringerPlus, 5(1160), 1–12.

Yolmeh, M., & Jafari, S. M. (2017). Applications of Response Surface Methodology in the Food Industry Processes. Food and Bioprocess Technology, 10(3), 413–433.

Yurekli, Y., Yildirim, M., Aydin, L., & Savran, M. (2017). Filtration and removal performances of membrane adsorbers. Journal of Hazardous Materials, 332, 33–41.

Zhao, D., Feng, J., Huo, Q., Melosh, N., Fredrickson, G. H., Chmelka, B. F., & Stucky, G. D. (1998). Triblock Copolymer Syntheses of Mesoporous Silica with Periodic 50 to 300 Angstrom Pores. Science, 279, 548–552.

Zhu, L., Ji, J., Wang, S., Xu, C., Yang, K., & Xu, M. (2018). Chemosphere Removal of Pb (II) from wastewater using Al 2 O 3 -NaA zeolite composite hollow fi ber membranes synthesized from solid waste coal fl y ash. Chemosphere, 206, 278–284.

Zolgharnein, J., Shahmoradi, A., & Ghasemi, J. B. (2013). Comparative study of Box-Behnken, central composite, and Doehlert matrix for multivariate optimization of Pb (II) adsorption onto Robinia tree leaves. Journal of Chemometrics, 27(1–2), 12–20.

ACHEVEMENTS

List of publications

1. Hasan, R., Chong, C. C., Bukhari, S. N., Jusoh, R., & Setiabudi, H. D. (2019). Effective removal of Pb(II) by low-cost fibrous silica KCC-1 synthesized from silica-rich rice husk ash. Journal of Industrial and Engineering Chemistry. 75, 2019, 262-270. https://doi.org/10.1016/j.jiec.2019.03.034

2. Hasan, R., & Setiabudi, H. D. (2019). Removal of Pb(II) from aqueous solution using KCC-1: Optimization by response surface methodology (RSM). Journal of King Saud University – Science. https://doi.org/10.1016/j.jksus.2018.10.005.

3. Hasan, R., Chong C.C., & Setiabudi, H.D. (2019) Synthesis of KCC-1 using rice husk ash for Pb removal from aqueous solution and petrochemical wastewater. Bulletin of Chemical Reaction Engineering & Catalysis, 14(1), 196-204. https://doi.org/10.9767/bcrec.14.1.3619.196-204

4. Hasan, R., Ahliyasah, N.A.F., Chong, C.C., Jusoh, R., & Setiabudi, H.D. (2019) Eggshell Treated Oil Palm Fronds (EG-OPF) as low-cost adsorbent for Methylene Blue Removal. Bulletin of Chemical Reaction Engineering & Catalysis, 14(1), 158-164. https://doi.org/10.9767/bcrec.14.1.3322.158-164

5. Hasan, R., Chong, C.C., Setiabudi, H.D., Jusoh, R., Jalil, A.A. (2019) Process optimization of methylene blue adsorption onto eggshell–treated palm oil fuel ash. Environmental Technology & Innovation, 13, 67-73. https://doi.org/10.1016/j.eti.2018.10.004.

6. Hasan, R., Razifuddin, N. A. M., Jusoh, N. W. C., Jusoh, R., & Setiabudi, H. D. (2018). Artocarpus integer peel as a highly effective low-cost adsorbent for methylene blue removal: Kinetics, isotherm, thermodynamic and pelletized studies. Malaysian Journal of Fundamental and Applied Sciences, 14(1), 25-31. https://doi.org/10.11113/mjfas.v14n1.791

Scopus Proceeding

1. Hasan, R., Bukhari, S. N., Jusoh, R., Mutamim, N. S. A., & Setiabudi, H. D. (2018). Adsorption of Pb(II) onto KCC-1 from aqueous solution: Isotherm and Kinetic study. Material Today: Proceedings, 5(10), 2018, 21574-21583. In conjuction with 3rd International Conference on Green Chemical Engineering and Technology 2017 (GCET), 7-8 November 2017, Swiss-Garden Hotel, Melaka, Malaysia (Oral presenter).

Exhibition

1. Herma Dina Setiabudi, Ruzinah Isha, Rohayu Jusoh, Rosalyza Hasan, Chong Chi Cheng. "Green Industrial Wastewater Treatment System". 2019 Creation, Innovation, Technology & Research Exposition (CITREX 2019), Universiti Malaysia Pahang, Pahang, Malaysia. 12-13 February 2019. (Gold & Best Invention in Fluid Award)